Los Alamos

NATIONAL LABORATORY

research note

Applied Physics Division, X-3
Computational Analysis and Simulation, X-3

To/MS: Distribution
From/MS: S. G. Mashnik, X-3, MS B283
Phone/FAX: 7-9946/7-1931
Email: mashnik@lanl.gov
Symbol: X-3-RN(U)06-07, LA-UR-06-1764
Date: March 6 2006

CEM03.S1, CEM03.G1, LAQGSM03.S1, and LAQGSM03.G1 Versions of CEM03.01 and LAQGSM03.01 Event Generators

Abstract

The latest versions of our event generators CEM03.01 and LAQGSM03.01 have been extended to describe production of light and medium fragments from various reactions. This was done in two different approaches: 1) By implementing into CEM03.01 and LAQGSM03.01 the **S**tatistical Multifragmentation Model (SMM) to consider multifragmentation as a mode competitive to evaporation of particles and light fragments, when the excitation energy U of a compound nucleus produced after the preequilibrium stage of a reaction is above $2 \times A$ MeV. This way, we have produced the "S" version of our codes ("S" stands for **S**MM), CEM03.S1 and LAQGSM03.S1. 2) By replacing the Generalized Evaporation Model GEM2 used in CEM03.01 and LAQGSM03.01 with the fission-like binary-decay model **G**EMINI, which considers production of all possible fragments. This way, we have produced the "G" version of our codes ("G" stands for **G**EMINI), CEM03.G1 and LAQGSM03.G1. This Research Note presents a summary and progress report on development of CEM03.S1, CEM03.G1, LAQGSM03.S1, and LAQGSM03.G1. This work was performed by S. G. Mashnik (X-3) in collaboration with K. K. Gudima and M. I. Baznat of the Academy of Science of Moldova, with important contribution and support from A. J. Sierk (T-16), R. E. Prael (X-3), and N. V. Mokhov of FNAL.

1. Introduction

For Proton Radiography (PRAD) as a radiographic probe for the Advanced Hydro-test Facility and other LANL applications, we have developed recently (see, e.g., [1]–[4] and references therein) improved versions of the Cascade-Exciton Model (CEM) [5] and of the Los Alamos Quark-Gluon String Model (LAQGSM) [6] codes as event generators to be used in MCNP6, MARS, and MCNPX transport codes.

The latest versions of the event generators, CEM03.01 and LAQGSM03.01, [7]–[9] have significantly improved Intra-Nuclear Cascade (INC) models, updated preequilibrium, Fermi Break-up, and coalescence models able to describe better than their predecessors emission of

complex particles and light fragments, and were extended to describe photonuclear reactions up to tens of GeV. On the whole, CEM03.01 and LAQGSM03.01 describe nuclear reactions much better than their predecessors and other similar codes available to the nuclear physics community. They have been benchmarked on a variety of particle-particle, particle-nucleus, and nucleus-nucleus reactions at energies from 10 MeV to 800 GeV per nucleon, and have have been or are being incorporated as event generators into the transport codes MCNP6, MARS, and MCNPX.

However, both CEM03.01 and LAQGSM03.01 still have some problems in a correct description of light and medium fragments produced from some nuclear reactions on medium-mass targets, which cannot fission or fragment into many channels using the GEM2 model. This problem is addressed in the work described here in two different ways:

1) By implementing into CEM03.01 and LAQGSM03.01 the **S**tatistical Multifragmentation Model (SMM) by Botvina *et al.* [10]–[14], to consider multifragmentation as a mode competitive to evaporation of particles and light fragments, when the excitation energy U of a compound nucleus produced after the preequilibrium stage of a reaction is above $2 \times A$ MeV. This way, we have produced the "S" version of our codes ("S" stands for **S**MM), CEM03.S1 and LAQGSM03.S1.

2) By replacing the Generalized Evaporation Model GEM2 of Furihata [15]–[17] used in CEM03.01 and LAQGSM03.01 with the fission-like binary-decay model **G**EMINI of Charity *et al.* [18]–[22] which considers production of all possible fragments. This way, we have produced the "G" version of our codes ("G" stands for **G**EMINI), CEM03.G1 and LAQGSM03.G1.

This Research Note presents a summary and progress report on development of CEM03.S1, CEM03.G1, LAQGSM03.S1, and LAQGSM03.G1. The INC, preequilibrium, Fermi Break-up, evaporation, and the coalescence models used in the current versions of our codes are described in detail in [4, 6, 7, 9] and references therein, therefore we do not discuss them here. Section 2 presents a short description of the Statistical Multifragmentation Model merged with our event generators, following [23]. Section 3 describes briefly the fission-like binary-decay model GEMINI. We have validated and verified our new codes CEM03.S1, LAQGSM03.S1, CEM03.G1 and LAQGSM03.G1 and have benchmarked them against a large variety of particle-nucleus and nucleus-nucleus measured reactions. Section 4 provides several examples of results obtained with our new codes compared with recent experimental data.

2. The Statistical Multifragmentation Model (SMM)

The multifragmentation model describes final states (nuclear fragments) as a process of break-up of highly excited nuclei, like an explosion [10]. At high excitation energies, when a nuclear system can eventually break up into several fragments, the multifragmentation mechanism may become dominant. The excited primary fragments produced via multifragmentation propagate independently in their mutual Coulomb field and undergo de-excitation. A detailed description of the multifragmentation mechanism can be found in the review [10]. The initial information

needed to calculate the multifragmentation stage of a reaction consists of the mass and charge numbers, A and Z, of the excited residual nucleus produced after the preequilibrium stage of a reaction, and its excitation energy U.

Multifragmentation Probability. The probability of a breakup channel b is given by the expression (in the so-called microcanonical approach [10, 11]):

$$W_b(U, A, Z) = \frac{1}{\sum_b \exp[S_b(U, A, Z)]} \exp[S_b(U, A, Z)], \tag{1}$$

where $S_b(U, A, Z)$ is the entropy of a multifragment state of the corresponding breakup channel b. The channels $\{b\}$ can be parameterized by a set of fragment multiplicities N_{A_f, Z_f} for fragments with mass numbers A_f and charges Z_f. All partitions $\{b\}$ should satisfy constraints derived from the total mass and charge conservation:

$$\sum_f N_{A_f, Z_f} A_f = A \tag{2}$$

and

$$\sum_f N_{A_f, Z_f} Z_f = Z. \tag{3}$$

It is assumed [11] that a thermodynamic equilibrium is established in every channel, which can be characterized by the channel temperature T_b. The channel temperature T_b is determined by the equation constraining the average energy $E_b(T_b, V)$ associated with the partition b:

$$E_b(T_b, V) = U + E_{ground} = U + M(A, Z), \tag{4}$$

where V is the system volume, E_{ground} is the ground state (at $T_b = 0$) energy of the system and $M(A, Z)$ is the mass of the nucleus. According to the conventional thermodynamics formulae, the average energy of a partition b is expressed through the system free energy F_b as

$$E_b(T_b, V) = F_b(T_b, V) + T_b S_b(T_b, V). \tag{5}$$

Thus, if the free energy F_b of a partition b is known, we can find the channel temperature T_b from Eqs. (4) and (5), then the entropy $S_b = -dF_b/dT_b$ and hence, the decay probability W_b defined by Eq. (1) can be calculated.

Calculation of the free energy is based on the liquid-drop description of individual fragments [11]. The free energy of a partition b can be split into several terms:

$$F_b(T_b, V) = \sum_f F_f(T_b, V) + E_C(V), \tag{6}$$

where $F_f(T_b, V)$ is the average energy of an individual fragment, including the volume

$$F_f^V = [-E_0 - T_b^2/\epsilon(A_f)]A_f, \tag{7}$$

surface

$$F_f^{Sur} = \beta_0[(T_c^2 - T_b^2)/(T_c^2 + T_b^2)]^{5/4} A_f^{2/3} = \beta(T_b)A_f^{2/3}, \tag{8}$$

symmetry

$$F_f^{Sim} = \gamma(A_f - 2Z_f)^2/A_f, \tag{9}$$

Coulomb

$$F_f^C = \frac{3}{5}\frac{Z_f^2 e^2}{r_0 A_f^{1/3}}[1 - (1 + \kappa_C)^{-1/3}], \tag{10}$$

and the translational

$$F_f^t = -T_b\left[\ln Z_{A_f,Z_f} - \ln(N_{A_f,Z_f}!)/N_{A_f,Z_f}\right] \tag{11}$$

terms. Using the Boltzmann gas approximation ($g_f = 1$ and the translational energy $E_b^t = 3/2T_b$), the translation partition sum can be calculates as follows:

$$Z_{A_f,Z_f} = g_f V_f \int \frac{d^3 p_{A_f,Z_f}}{(2\pi\hbar)^4} \exp\left[-\frac{p_{A_f,Z_f}^2}{2m_{A_f,Z_f}T}\right] = g_f V_f \left(\frac{2m_{A_f,Z_f}}{2\pi\hbar^2}\right)^{3/2}. \tag{12}$$

The expression for the translational free energy can be approximated further, if to assume that $m_{A_f,Z_f} = m_N A_f$, where m_N is the nucleon mass and $N_{A_f,Z_f}! \approx (\frac{N_{A_f,Z_f}}{e})_{A_f,Z_f}^N$. We can introduce the thermal wavelength $\lambda_{T_b} = (2\pi\hbar^2/m_N T_b)^{1/2}$ and rewrite Eq. (11) as following:

$$F_f^t = -T_b\left(\ln\frac{V_f A_f^{3/2}}{\lambda_{T_b}^3 N_{A_f,Z_f}} + 1\right). \tag{13}$$

The last term in Eq. (6),

$$E_C(V) = \frac{3}{5}\frac{Z^2 e^2}{R}, \tag{14}$$

is the Coulomb energy of a uniformly charged sphere with the charge Ze and the radius $R = (3V/4\pi)^{1/3} = r_0 A^{1/3}(1 + \kappa_C)^{1/3}$, where $\kappa_C = 2$ [11]. The parameters $E_0 = 16$ MeV, $\beta_0 = 18$ MeV, and $\gamma = 25$ MeV are coefficients of the Bethe-Weizsacker formula at $T_b = 0$. $g_f = (2S_f + 1)(2I_f + 1)$ is spin, S_f, and isospin, I_f, degeneracy factor for a fragment. Fragments with $A_f > 1$ are treated as Boltzmann particles. $T_c = 18$ MeV is the critical temperature, which corresponds to the liquid-gas phase transition, and $r_0 = 1.17$ fm. $\epsilon(A_f) = \epsilon_0[1 + 3/(A_f - 1)]$ is the inverse level density of the mass A_f fragment and $\epsilon_0 = 16$ MeV is considered as a variable model parameter, whose value depends on the fraction of energy transferred to the internal degrees of freedom of fragments [11]. The free volume $V_f = \kappa V = \kappa\frac{4}{3}\pi r_0^4 A$ available to the translational motion of a fragment, where $\kappa \approx 1$, and its dependence on the multiplicity of fragments can be taken from [11]:

$$\kappa = \left[1 + \frac{1.44}{r_0 A^{1/3}}(M^{1/3} - 1)\right]^3 - 1, \tag{15}$$

with $\kappa = 0$, if $M = 1$. The light fragments with $A_f < 4$, which have no excited states, are considered as elementary particles characterized by empirical masses M_f, radii R_f, binding energies B_f, and spin degeneracy factors g_f of the ground states, respectively. They contribute to the free translation and Coulomb energies.

Direct Simulation of the Low Multiplicity Multi-fragment Disintegration. At comparatively low excitation energies (temperatures), the system will disintegrate into a small number of fragments $M \leq 4$ and the number of channels is not big. In such situations, a direct (micro-canonical) sorting of all decay channels can be performed. Then, using Eq. (1), the average multiplicity value $< M >$ can be found. To check that we have really a situation with low excitation energy, the obtained value of $< M >$ is examined to obey the inequality $< M > \leq M_0$, where $M_0 = 3.3$ and 2.6 for $A \sim 100$ and ~ 200, respectively [11]. If the discussed inequality is fulfilled, then the set of channels under consideration is believed to be suitable for a correct description of the break up. Then, using probabilities calculated according to Eq. (1), we can select randomly a specific channel with given values of A_f and Z_f.

Fragment Multiplicity Distribution. The individual fragment multiplicities N_{A_f,Z_f} in the so-called macro-canonical ensemble [10] are distributed according to the Poisson distribution:

$$P(N_{A_f,Z_f}) = \exp\left(-\omega_{A_f,Z_f}\right)\frac{\omega_{A_f,Z_f}^{N_{A_f,Z_f}}}{N_{A_f,Z_f}!} \, , \tag{16}$$

with mean value $< N_{A_f,Z_f} > = \omega_{A_f,Z_f}$ defined as

$$< N_{A_f,Z_f} > = g_f A_f^{3/2} \frac{V_f}{\lambda_{T_b}^3} \exp\left[\frac{1}{T_b}(F_f(T_b,V) - F_f^t(T_b,V) - \mu A_f - \nu Z_f)\right], \tag{17}$$

where μ and ν are chemical potentials. The chemical potentials can be found by substituting Eq. (17) into the system of constraints:

$$\sum_f < N_{A_f,Z_f} > A_f = A \tag{18}$$

and

$$\sum_f < N_{A_f,Z_f} > Z_f = Z \tag{19}$$

and solving them by iteration.

Fragment Mass Number Distribution. Fragment mass numbers $A_f > 1$ are distributed also according to the Poisson distribution [10] (see Eq. (16)) with the mean value $< N_{A_f} >$ defined as

$$< N_{A_f} > = A_f^{3/2} \frac{V_f}{\lambda_{T_b}^3} \exp\left[\frac{1}{T_b}(F_f(T_b,V) - F_f^t(T_b,V) - \mu A_f - \nu < Z_f >)\right], \tag{20}$$

where one has to substitute $Z_f \rightarrow < Z_f >$ while calculating the internal free energy $F_f(T_b, V) - F_f^t(T_b, V)$. The average charge $< Z_f >$ of fragments with the mass number A_f is given by

$$< Z_f(A_f) > = \frac{(4\gamma + \nu)A_f}{8\gamma + 2[1 - (1 + \kappa)^{-1/3}]A_f^{2/3}} \ . \tag{21}$$

Fragment Charge Distribution. For a given mass of fragments, $A_f > 1$, the charge Z_f distribution of fragments is described by a Gaussian distribution:

$$P(Z_f(A_f)) \sim \exp\left[-\frac{(Z_f(A_f) - < Z_f(A_f) >)^2}{2(\sigma_{Z_f}(A_f))^2}\right] , \tag{22}$$

with a variance

$$\sigma_{Z_f(A_f)} = \sqrt{\frac{A_f T_b}{8\gamma + 2[1 - (1 + k)^{-1/3}]A_f^{2/3}}} \approx \sqrt{\frac{A_f T_b}{8\gamma}} \ . \tag{23}$$

and the average charge $< Z_f(A_f) >$ is defined by Eq. (21).

Fragment Kinetic Energy Distribution. It is assumed [11] that at the instant of nucleus break-up, the kinetic energy of the fragment T_{kin}^f in the rest frame of the nucleus obeys the Boltzmann distribution at a given temperature T_b:

$$\frac{dP(T_{kin}^f)}{dT_{kin}^f} \sim \sqrt{T_{kin}^f} \exp\left(-T_{kin}^f/T_b\right) \ . \tag{24}$$

Assuming a thermodynamic equilibrium, the fragments have isotropic velocity distributions in the rest frame of the nucleus. The total kinetic energy of fragments should be equal to $\frac{3}{2}MT_b$, where M is the multiplicity of fragments. The total momentum of all fragments should be equal to zero. These conditions are fulfilled by a proper choice of the momenta of the last two simulated fragments. The initial conditions for the divergence of the fragment system are determined by a random selection of fragment coordinates distributed with equal probabilities over the break-up volume $V_f = \kappa V$ (it can be a sphere or a prolonged ellipsoid). Then, the Newton's equations of motion can be solved for all fragments in a self-consistent time-dependent Coulomb field [11]. Thus, the asymptotic energies of fragments determined as a result of this procedure differ from the initial values by the Coulomb repulsion energy.

Fragment Excitation Energies. The temperature T_b determines the average excitation energy of each fragment:

$$U_f(T_b) = E_f(T_b) - E_f(0) = \frac{T_b^2}{\epsilon_0}A_f + \left[\beta(T_b) - T_b\frac{d\beta(T_b)}{dT_b} - \beta_0\right]A_f^{2/3}, \tag{25}$$

where $E_f(T_b)$ is the average fragment energy at a given temperature T_b, and $\beta(T_b)$ is defined by Eq. (8). No excitation energy is considered for fragment with $A_f < 4$; for ^4He, the excitation energy can be taken as $U_{^4He} = 4T_b^2/\epsilon_o$.

Monte-Carlo Simulation Procedure. We merged with our CEM03.01 and LAQGSM03.01 event generators the SMM code as kindly provided by its author, Dr. Botvina, to one of us (KKG), without any essential changes or fitting of its parameter. In both our codes, we consider multifragmentation as a possible mechanism of nuclear reactions only when the excitation energy of the nuclei formed after the preequilibrium stage is higher than $2 \times A$ MeV.

The SMM Monte-Carlo simulation of fragment characteristics can be outlined as follows:

1) Perform a direct simulation of the low-multiplicity disintegration using Eq. (1) and find the average multiplicity value $< M >$. Verify that the value of $< M >$ found is really small, *i.e.*, $< M > \leq M_0$. Using probabilities calculated according to Eq. (1), select randomly a specific channel with given values of A_f and Z_f. Then proceed to the step #5. If the value of $< M >$ obtained is $> M_0$, proceed to the next step (#2).

2) Sample the mass numbers of the fragments, A_f^i, where $1 \leq A_f^i \leq A$ according to the Poisson distribution, Eq. (16), with the mean value $< N_{A_f} >$ defined by Eq. (20).

3) For randomly chosen values of A_f^i according to the Gaussian distribution, Eq. (22), with a variance defined by Eq. (23) and the average $< Z_f(A_f) >$ defined by Eq. (21), select the fragment charge Z_f^i, where $0 \leq Z_f^i \leq Z$.

4) Repeat the sampling procedure of A_f^i (step #2) and Z_f^i (step #3) i times, until the mass and charge numbers of all fragments are defined. If the sum of nucleons and the charge of all fragments exceed the values of A and Z, the procedure should be repeated starting from $i = 1$ at the step #2.

5) For randomly chosen values of A_f and Z_f, determine the fragment kinetic energies T_{kin}^f at the instant of the nucleus break-up in the rest frame of the decaying nuclear system using Eq. (24). Then, define the fragment velocities and momenta, assuming an isotropic distribution of velocities in the rest frame of the decaying nucleus. Use the momenta of the two last fragments to fulfill energy-momentum conservation. Via a random selection of fragment coordinates distributed with equal probabilities over the break-up volume $V_f = \kappa V$, determine the initial conditions for the divergence of the fragment system after the break-up instant. Solve Newton's equations of motion for all fragments in the self-consistent time-dependent Coulomb field, to define the asymptotic energies of the fragments.

6) Calculate the excitation energy of the fragments using Eq. (25).

3. The Binary-Decay Evaporation/Fission Code GEMINI

The code GEMINI calculates the decay of compound nuclei by fission-like sequential binary decays. All possible binary divisions from light-particle emission to symmetric division are considered. The code employs the Monte-Carlo technique to follow the decay chains of individual compound nuclei through sequential binary decays until the resulting products are unable to undergo further decay.

The decay width for the evaporation of fragments with $Z \leq 2$ is calculated using the Hauser-Feshbach formalism [25]. For the emission of a light particle (Z_1, A_1) of spin J_1, from a system (Z_0, A_0) of excitation energy E^* and spin J_0, leaving the residual system (Z_2, A_2) with spin J_2, the decay width is given by:

$$\Gamma(Z_1, A_1, Z_2, A_2) = \frac{2J_1 + 1}{2\pi\rho_0} \sum_{l=|J_0-J_2|}^{J_0+J_2} \int\limits_{0}^{(E^*-B-E_{rot}(J_2))} T_l \rho_2(U_2, J_2) d\epsilon . \tag{26}$$

In this equation, l and ϵ are the orbital angular momentum and kinetic energy of the emitted particle, $\rho_2(U_2, J_2)$ is the level density of the residual system with thermal excitation energy

$$U_2 = E^* - B - E_{rot}(J_2) - \epsilon . \tag{27}$$

B is the binding energy, $E_{rot}(J_2)$ is the rotational plus deformation energy of the residual system, and ρ_0 is the level density of the initial system.

The transmission coefficients $T_l(\epsilon)$ are calculated with the sharp cut-off approximation for a classical system of absorptive radius R, and are given by:

$$T_l(\epsilon) = \begin{cases} 0, & \text{for} \quad \epsilon < E_{Coul} + \dfrac{\hbar^2 l(l+1)}{2\mu R^2} , \\[4mm] 1, & \text{for} \quad \epsilon \geq E_{Coul} + \dfrac{\hbar^2 l(l+1)}{2\mu R^2} , \end{cases} \tag{28}$$

where μ is the reduced mass. The Coulomb barriers E_{Coul} are calculated using the empirical expressions of Vaz and Alexander and the absorptive radius is taken as

$$R = \begin{cases} 1.16 A_2^{1/3} + 2.6 \text{ fm}, & \text{for proton and neutron emission}, \\ 1.16 A_2^{1/3} + 3.7 \text{ fm}, & \text{for } \alpha \text{ particle emission}. \end{cases} \tag{29}$$

In calculating the binding energy for heavy systems $(A > 12)$, the masses of the initial and residual systems were obtained from the Yukawa-plus-exponential model of Krappe, Nix, and Sierk [26] without the shell and pairing correction terms. The parameters for this model are taken from the more recent fit to experimental masses of Moller and Nix [27]. These separation energies are expected to be more appropriate at high excitation energies where shell and pairing effects are predicted to wash out. For very light systems $(A \leq 12)$, binding energies are calculated from the experimental masses. The rotational plus deformation energy E_{rot} of a nucleus was taken from the Rotating Finite-Range Model (RFRM) calculations of Sierk [28].

For binary divisions corresponding to the emission of heavier fragments, the decay width is calculated using the transition-state formalism of Moretto [24].

$$\Gamma(Z_1, A_1, Z_2, A_2) = \frac{1}{2\pi\rho_0} \int\limits_{0}^{(E^*-E_{sad}(J_0))} \rho_{sad}(U_{sad}, J_0) d\epsilon , \tag{30}$$

where U_{sad} and ρ_{sad} are the thermal energy and level density of the conditional saddle-point configuration,

$$U_{sad} = E^* - E_{sad}(J_0) - \epsilon \ . \tag{31}$$

$E_{sad}(J_0)$ is the deformation plus rotation energy of the saddle-point configuration and ϵ now is the kinetic energy of the translational degree of freedom.

The deformation plus rotation energy is calculated with the RFRM using a two-spheroid parameterization for the shape of the conditional saddle-point configuration. This parameterization results in conditional barriers which are within 2 MeV of saddle-point energies calculated with more realistic shape parameterizations for $A_0 = 110$ [28]. Better agreement is obtained for lighter nuclei. To correct for this difference to first order, the two-spheroid saddle-point energies are scaled by a constant factor for all mass asymmetries and angular momentum. The scaling factor is chosen so that for symmetric division, the scaled saddle-point energy is equal to the value calculated with the more realistic shape parameterization by Sierk [28, 29]. For $Z \leq 6$, these RFRM saddle-point energies $[E^{\mathrm{RFRM}}(J_0)]$ are modified by

$$E_{sad}(J_o) = E^{\mathrm{RFRM}}(J_0) - M_{\mathrm{Y+e}}(Z_1, A_1) + M_{exp}(Z_1, A_1) \ , \tag{32}$$

where $M_{\mathrm{Y+e}}$ is the mass predicted by the Yukawa-plus-exponential model without shell and pairing corrections and M_{exp} is the experimental mass. This modification is an attempt to introduce shell effects into the saddle-point energies for very asymmetric divisions, where one expects them to become more important.

For all level densities, the Fermi-gas expression

$$\rho(U, J) = (2J + 1) \left[\frac{\hbar^2}{2\Im} \right]^{\frac{3}{2}} \frac{\sqrt{a}}{12} \frac{\exp 2\sqrt{aU}}{U^2} \tag{33}$$

is used, where the J is the moment-of-inertia of the residual nucleus at the saddle-point configuration. The level-density parameter is taken here as $a = A/8.5$ MeV^{-1} for both the residual nucleus and in saddle-point configurations.

The integrations in Eqs. (26) and (30) are performed by first expanding the integrand around the lower limit, giving the approximate expression for the decay width for $Z_1 \leq 2$ as

$$\Gamma(Z_1, A_1, Z_2, A_2) = \frac{2J_1 + 1}{2\pi\rho_0} \sum_{J_2=0}^{\infty} \sum_{l=(J_0-J_2)}^{(J_0+J_2)} t_2 \rho_2(U_2, J_2) \ , \tag{34}$$

where now:

$$U_2 = E^* - B - E_{rot}(J_2) - E_{Coul} - \frac{\hbar^2 l(l+1)}{2\mu R^2} \ , \tag{35}$$

and the nuclear temperature is approximately:

$$t_2 = \sqrt{\frac{U_2}{a}} \ . \tag{36}$$

For $Z_1 > 2$

$$\Gamma(Z_1, A_1, Z_2, A_2) = \frac{1}{2\pi\rho_0} t_{sad} \rho_{sad}(U_{sad}, J_0) \ , \tag{37}$$

where now:

$$U_{sad} = E^* - E_{sad}(J_0) \ , \tag{38}$$

and the temperature of the saddle-point configuration is approximately:

$$t_{sad} = \sqrt{\frac{U_{sad}}{a}} \ . \tag{39}$$

The secondary products formed in the binary decay of the initial system, (Z_1, A_1) and $Z_2, A_2)$, are allowed to undergo sequential binary decay. The spin of the residual system is chosen in a Monte-Carlo fashion from the calculated partial decay widths $\Gamma_{J_2}(Z_1, A_1, Z_2, A_2)$. Its excitation energy is calculated as

$$E_2^* = U_2 - 2t_2 + E_{rot}(J_2) \ . \tag{40}$$

For $Z > 2$, the spin of the fragments is calculated in the sticking limit, *i.e.*, for fragment 1

$$J_1 = (\frac{\Im_1}{\Im})J_0 \ , \tag{41}$$

where $\Im_1$ is the moment of inertia of the fragment and $\Im$ is the total moment of inertia of the system. Its excitation energy is derived assuming equal temperatures for the two fragments,

$$E_1^* = \frac{A_1}{A_0}[U_{sad} - t_{sad}] + E_{rot}(J_1) \ . \tag{42}$$

This is strictly valid only when the saddle- and scission-point configurations are degenerate and this is approximately true for the systems studied in this work. However, Eq. (42) is not applicable for heavier systems.

GEMINI Code Description. We have merged with our event generators the standard version of the code GEMINI, as kindly provided by its author, Prof. Charity, to one of us (AJS), without any essential changes or fitting of its parameters.

GEMINI follows the decay chain of a compound nucleus via sequential binary decays. The conditional barriers used in the statistical decay width for $A < 100$ are obtained from a two-spheroid finite-range program written by A. J. Sierk. For $100 < A < 190$, the barriers are extrapolated from calculations of Sierk using more shape parameters to obtain the conditional-saddle-point energy.

Angle and velocities of all the fragments can be calculated in two different ways:

1) Semi-classical treatment of emission angles and velocities and spin orientations (faster option);

2) Quantum treatment of spin projections, *i.e.*, choose the m values for each J. This option also gives quantum angular distributions. Note that both options are approximations and have their limitations.

We list below several important features of GEMINI as provided by its author, Prof. Charity, in his comments for users:

A) *Semi-Classical Approach for Evaporation:* From the quantum mechanical numbers chosen in evaporation subroutines, classical vectors are determined. In the original version, the angle of the evaporated particle is always chosen perpendicular to the particle's orbital angular momentum vectors. This, however, is only a good approximation for high angular momentum, and as most evaporated particles are emitted at low angular momentum, it produces too much emission in the reaction plane. For the later version, the angle of emission relative to orbital angular momentum vector is obtained from the quantum distribution for $m = 1$.

B) *Quantum Treatment for Evaporation:* At each stage in the decay sequence, the "m" quantum numbers (angular momentum projection) are chosen for each angular momentum vector from the probabilities given by the square of Clebsch-Gordon coefficients. Once the m values are selected, the emission-angle distribution is obtained from the square of the appropriate associated Legendre polynomial, the φ angles are always random. In the original version, the initial compound nucleus spin was assumed to be $m = 0$ with quantization axis being the beam axis. This treatment is similar to that used by other evaporation codes such as EVAP. However, as all interference terms have been neglected in choosing the angle, there is no memory of the reaction plane, *i.e.* the φ angles are all random. As an alternative to this treatment, in the latest version the initial value of the compound nucleus spin projection is taken as $m = j$. Subsequently, all center-of-mass velocity vectors are rotated by $\Theta = 90°$ and in φ by a single random angle. This produces almost identical angular distributions to the original treatment, but now the φ angles are no longer random but show some memory of the reaction plane, if the initial angular momentum is large.

C) *Fission and Intermediate-Mass Fragment (IMF) Parameters:* GEMINI includes two possibilities: 1) the fission mode which is appropriate for prediction of cross sections, which however does not lead to a prediction for the mass-asymmetry distribution; 2) the IMF decay mode, where the Moretto's formalism [30, 31] of asymmetric divisions is considered.

D) *Choice of the Dividing Line Between Evaporation and IMF Emission (Z_{min}):* If $Z < Z_{min}$, the fragments are treated in routines with Hauser-Feshbach formalism; for $Z \geq Z_{min}$, the fragments are treated as IMF with the transition-state formalism.

E) *Level Density:* Many parameterizations of the level densities are possible: constant level-density parameter $a = A/a_0$, Toke and Swiatecki level density parameters [32], Ignatyuk *et al.* level density parameters [33], Gottschalk and Ledergerber level density parameters [34], and Lestone's temperature dependent level density parameters [35].

F) *Variance Reduction:* Complex fragment decays can be very improbable events. Thus, in a normal Monte-Carlo simulation one may have to run a large number events to achieve reasonable statistics for intermediate-mass fragments. To solve this problem, to some extent, weighting has been introduced into the program.

G) *Delay Time:* A time-delay parameter is included in GEMINI. All complex-fragment channels are delayed by the same amount. Fission and IMF decay is inhibited for a time $t_{delay}(\eta) = t_{delay} \times \exp(-\eta^2/(2\sigma_{delay}^2)) \times 1.0E^{-21}$ seconds, where the t_{delay} and σ_{delay} are parameters and $\eta = (A_2 - A_1)/(A_2 + A_1)$.

4. Results

1) We have incorporated GEMINI and SMM into CEM03.01 and LAQGSM03.01 as provided us by their authors, Prof. Charity and Dr. Botvina, without any essential changes to or fitting of their parameters. A few "cosmetic" changes we made were only to accommodate them to our FORTRAN compilers and to fix several observed "bugs".

2) We have verified, validated, and benchmarked the new CEM03.S1, CEM03.G1, LAQGSM03.S1, and LAQGSM03.G1 versions of our CEM03.01 and LAQGSM03.01 event generators against a variety of measured reactions and results by other models.

3) To understand better different mechanisms of final isotope production, we have analyzed many characteristics of various proton- and nucleus-induced nuclear reactions with all versions of our codes, "S", "G", and the standard one, "03.01". Several examples of this part of our work are presented below.

4) We have "frozen" the "G" and "S" versions of CEM03.01 and LAQGSM03.01 on several X-3 and T-16 computers. These versions are to be used as stand-alone codes or as event generators in working versions of transport codes MCNP6, MARS, and MCNPX, when we are interested in the production of light and medium fragments from targets not normally allowed to fission.

The upper-left plot in Fig. 1 shows the recent experimental data [36] on the mass-number distribution of the product yield from the reaction 660 MeV p + ^{129}I compared with results by the standard version of our CEM03.01 event generator, as well as with results by our new "S" and "G" codes (similar results were obtained for this reaction with LAQGSM03.01 and its "S" and "G" versions). One can see that the standard versions of our codes do not describe production of isotopes with mass number $26 < A < 63$ from this reaction observed in the experiment [36]: These products are too heavy to be evaporated from compound nuclei and the target is too light to fission, producing these isotopes as fission fragments (CEM03.01 and LAQGSM03.01 consider only "conventional" fission of preactinides and actinides and do not consider at all fission of nuclei with $Z < 65$).

The new "S" and "G" versions do predict such isotopes and agree reasonably well with available experimental data. This is the main reason we have developed the "S" and "G" versions of our codes. The results by the "S" version for the A-distribution of product yield are very similar to the ones from the "G" version for the entire range of product masses, except the region of light fragments $10 < A < 20$, where there are no experimental data. From this plot we see only that products with $26 < A < 63$ are produced in this reaction and they can be described either via fission-like binary decays (the "G" versions of our codes), or as products of multifragmentation of highly-excited nuclei (the "S" versions), without a distinctive preference.
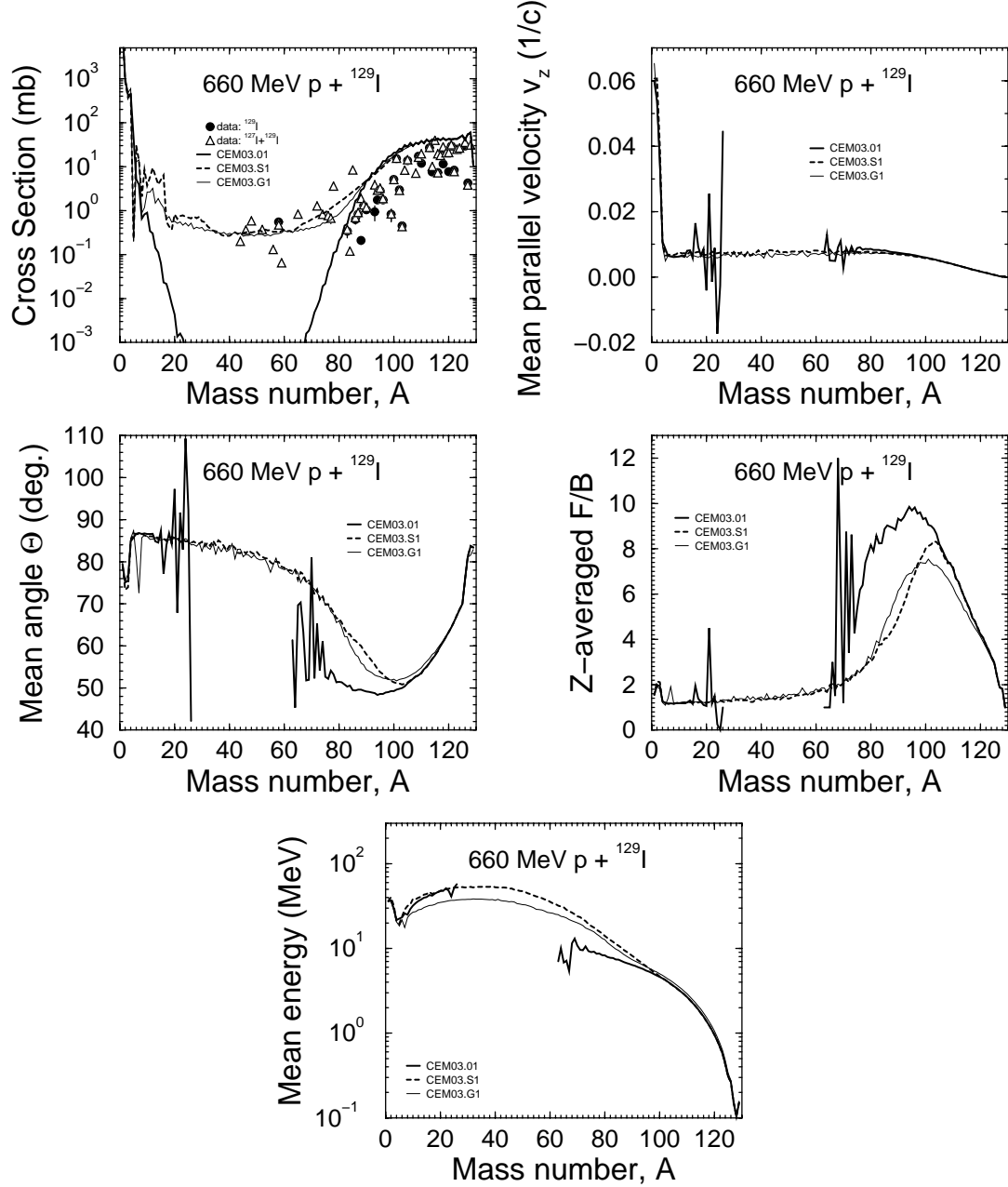
Figure 1: Predictions of CEM03.01, CEM03.S1, and CEM03.G1 for the mass number distribution of the product yield, mean parallel velocity v_z, mean production angle Θ, Z-averaged A-dependence of the F/B ratio of the forward product cross sections to the backward ones, and the mean kinetic energy of all products in the laboratory system for the reaction 660 MeV p + ^{129}I (lines) compared with available experimental data (symbols) [36], as indicated. The big fluctuations in the values by CEM03.01 of $< v_z >$, $< \Theta >$, $< R = F/B >$, and $< T_{kin} >$ for masses around $A = 20$ and 65 do not provide real physical information, as they are related to the limited statistics of our Monte-Carlo simulation caused by the very low yield of isotopes at the border between spallation and fragmentation, and at that between fragmentation and evaporation (with no events at all in the fragmentation region, $26 < A < 63$, neglected by CEM03.01). Our calculation provides only a few (or even one) isotopes of a given A in these mass regions, and mean values for such events do not have any significance.

With a hope to understand better the mechanisms of the production of isotopes with $26 < A < 63$ and of other products as well, we have also calculated with all versions of our codes several so called "recoil properties" of products, like the mean parallel velocity v_z, $< v_z >$, the mean production angle Θ, $< \Theta >$, Z-averaged A-dependence of the F/B ratio of the forward product cross sections to the backward ones, $< R >$, and the mean kinetic energy of all products in the laboratory system, $< T_{kin} >$, showed in other plots of Fig. 1. Such characteristics can be measured with some specific techniques for some nuclear reactions and have proven to be very useful in understanding reaction mechanisms [4], although the activation technique of the experiment [36] does not provide such measurements. On can see a big difference between results provided by the standard version, CEM03.01, and the "S" and "G" versions for $< \Theta >$, $< R >$, and $< T_{kin} >$ of products with $70 < A < 100$. We see also a significant difference between predictions by the "S" and "G" version for $< \Theta >$ of products with $85 < A < 110$, for $< R >$ of the same products, and for $< T_{kin} >$ of products with $15 < A < 80$. Unfortunately, none of these characteristics were measured and we can not make a preference for a specific reaction mechanism based on these results, until reliable experimental data are available.

Fig. 2 shows results similar to the ones presented in Fig. 1, only for a lighter target, ^{56}Fe, and a lower energy of 300 MeV measured in inverse kinematics at GSI as 300 MeV/nucleon ^{56}Fe + p [37, 38]. The situation with the agreement or disagreement of our calculations with the data [37, 38] is very similar to what we have in Fig. 1, and all comments here are the same: The standard versions of our event generators strongly underestimate production of fragments with $A < 32$ from this reaction. These fragments can be described either via fission-like binary decays (the "G" versions of our codes), or as products of multifragmentation of highly-excited nuclei (the "S" versions). Comparing only the total production cross sections with experimental data (Fig. 2, for Z-integrated A-dependence of the yield, and Fig. 3, where we show cross sections of all measured isotopes, separately) does not allow us to identify the "real" nuclear reaction mechanisms for the production of these isotopes. The so called "recoil properties" of products discussed above, like $< \Theta >$, $< R >$, and $< T_{kin} >$ are predicted differently by different models and could be more informative to study mechanisms of nuclear reactions, but such characteristics were not measured also by the GSI inverse-kinematics technique [37, 38]. Note, that in addition to the production cross section, the GSI inverse-kinematics technique provides also the mean parallel velocity v_z of all products in the reference frame of the projectile. As we can see from the upper-right plot of Fig. 2, $< v_z >$ is not sensitive enough to the reaction mechanisms, and all three versions of our codes, "S", "G", and the standard version "03.01" provide almost the same $< v_z >$, for this particular reaction. The mean kinetic energy of products is more sensitive to the reaction mechanisms considered, therefore more informative. As one can expect in advance, the multifragmentation mechanism ("S" version of our codes) provides more energetic light fragments (see the upper plots in Fig. 4, for $Z = 3, 6, 9, 12,$ and 15) than the fission-like binary decay model GEMINI ("G" version) and the "conventional" evaporation model considered by our standard "03.01" version do. With increasing
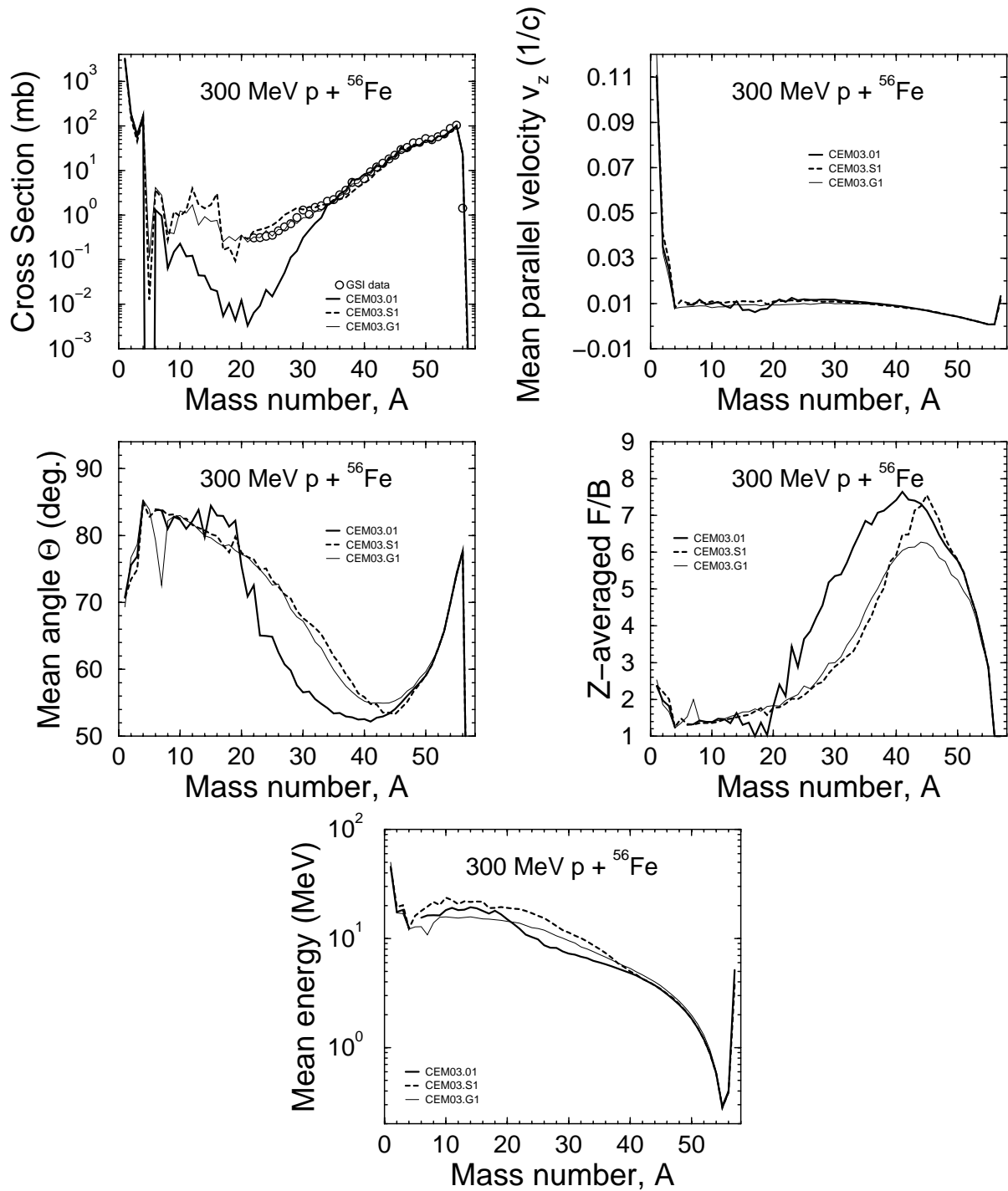
Figure 2: The same as in Fig. 1, but for the reaction 300 MeV p + ^{56}Fe measured at GSI in inverse kinematics [37,38].
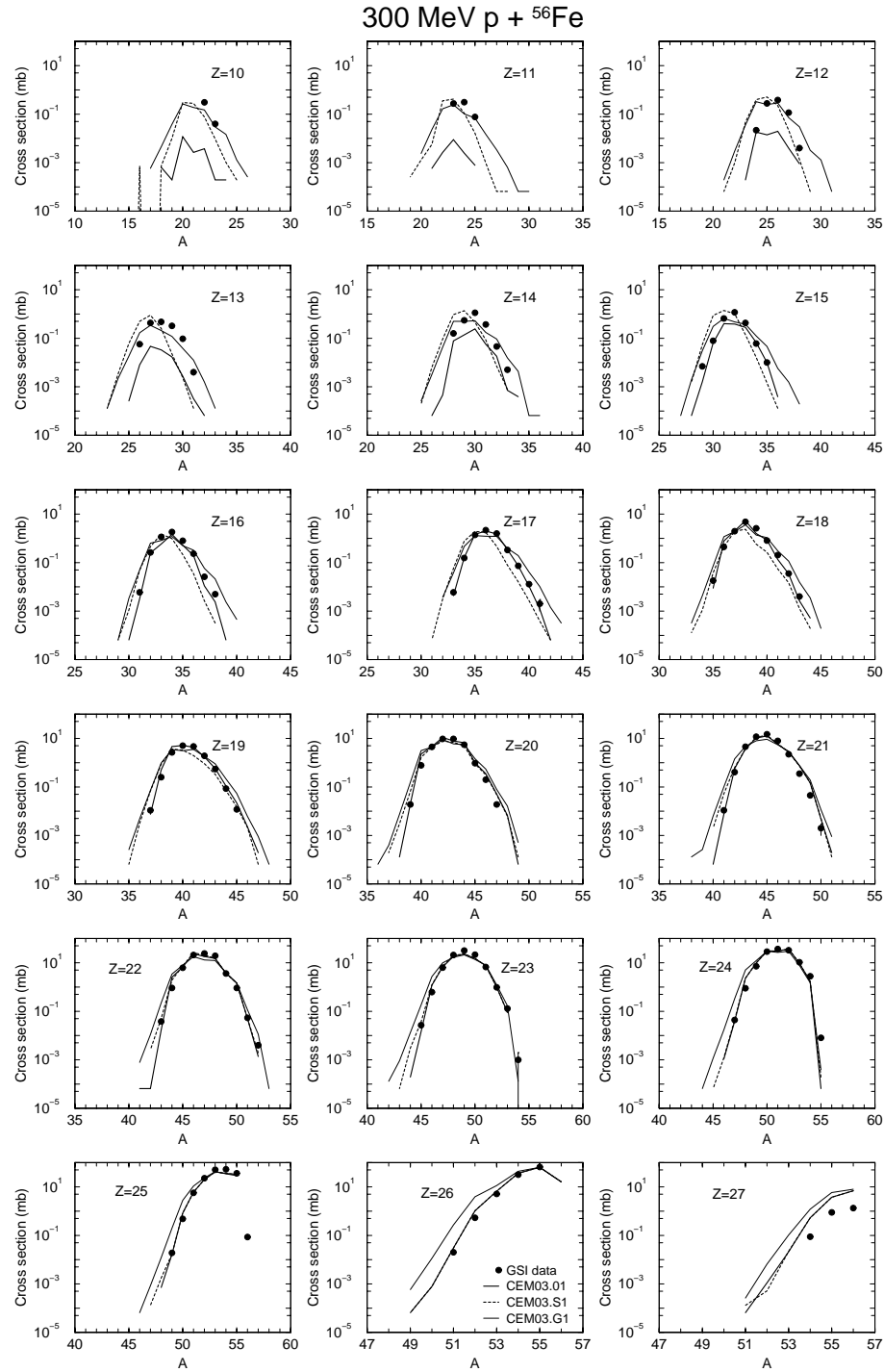
300 MeV p + ^{56}Fe

Figure 3: Comparison of all measured [37,38] cross sections (symbols) of products from the reaction 300 MeV p + ^{56}Fe with CEM03.01, CEM03.S1, and CEM03.G1 results (lines), as indicated.

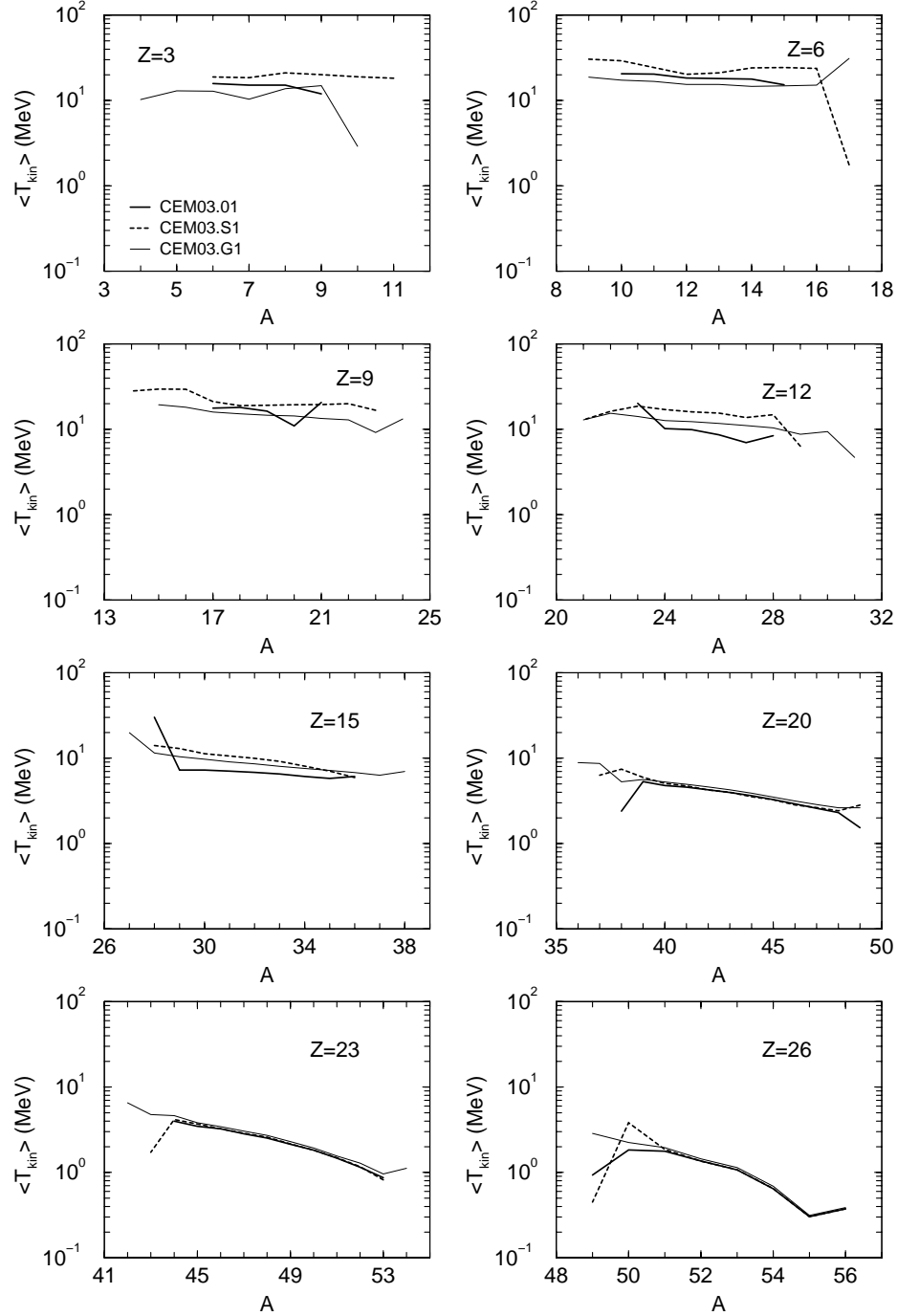## 300 MeV p + ^{56}Fe

Figure 4: Predictions by CEM03.01, CEM03.S1, and CEM03.G1 for the mean kinetic energy of eight nuclides with $Z = 3$, 6, 9, 12, 15, 20, 23, and 26 produced in the reaction 300 MeV p + ^{56}Fe (no experimental data are available to us). The big fluctuations in the values of $< T_{kin} >$ at both ends of distributions do not provide real physical information, as they are related to the limited statistics of our Monte-Carlo simulation caused by the very low yield of extremely neutron-rich and neutron-deficient isotopes. Our calculation provides only a few (or even one) isotopes of a given A in these regions, and mean values for such events do not have any significance.

mass/charge of the products, this difference diminishes, and for isotopes with $Z \geq 20$, all three versions of our codes predict the same values of $< T_{kin} >$ (lower plots in Fig. 4). Unfortunately, we do not have experimental data for such "recoil characteristics" of this reaction, therefore are not able to make an unambiguous choice between multifragmentation and binary decays in the production of light fragments from this reaction.

Figs. 5–7 provide results for the same reaction and very similar to the ones shown in Figs. 2–4, but for a higher energy of 1 GeV, also measured in inverse kinematics at GSI by Carmen Villagrasa *et al.* [37, 38] and by Paolo Napolitani *et al.* [39, 40]. At 1 GeV (Figs. 5–7), the situation changes a little in comparison with what we have above at 300 MeV: The energy here is higher and the reaction is deeper, the target, ^{56}Fe, is not too heavy, so, the standard version of our codes describe reasonably well all the measured product yields. At 1 GeV, the standard versions of our models predict light fragment production via deep spallation processes of INC followed by preequilibrium and evaporation, without considering the multifragmentation ("S" version) or/and binary-decay processes ("G" version). It is interesting that at 1 GeV, the standard "03.01" event generators describe these cross sections measured at GSI even better than the "S" or "G" versions do, especially for products with $5 < A < 16$ (see the upper-left plot in Fig. 5) and $Z < 10$ (see Fig. 6). However, we consider this fact only as natural result of several years of careful development of our standard event generators rather than an indication that no multifragmentation or/and binary decays occur at 1 GeV (from a physical point of view, if we have multifragmentation or/and binary decays at 300 MeV, one may expect to have them even more pronounced at 1 GeV): Our standard event generators CEM03.01 and LAQGSM03.01 consider the INC, preequilibrium, evaporation, and the coalescence models for the production of isotopes from this reaction, and each of these models have their own parameters. These parameters have been adjusted, then fixed, while developing CEM03.01 and LAQGSM03.01 so that our codes describe as well as possible arbitrary nuclear reactions. The "G" and "S" versions were produced here without any fitting or adjustment of any parameters. We think that by adjusting and fitting the parameters of the "G" and "S" versions, one may obtain an agreement of their results for the production cross sections not worse that the one provided by the standard version of our codes. A difference would be observed for predictions of other characteristics of reactions, like the so called "recoil properties" of products discussed above. In the framework of the versions we have so far, the biggest difference between results for this reaction by the "S", "G", and the standard "03.01" versions is for $< \Theta >$ and $< R >$ for products with $12 < A < 40$, for $< T_{kin} >$ of products with $5 < A < 30$, and we see also quite a big difference in the Z-integrated A-dependence of the yield for light fragments with $5 < A < 18$ (see the upper-left plot in Fig. 5).

We note that the GEM2 evaporation/fission model [15]–[17] does not consider the angular momenta of the emitted particles, therefore the angular momenta of nuclei calculated at the INC and preequilibrium stages of reactions are not used at all and neglected in evaporation and fission processes. The same is true for the "S" version of our codes. On the other hand, GEMINI [18]–[22] does consider angular momenta of all products, so the "G" version of our codes can be
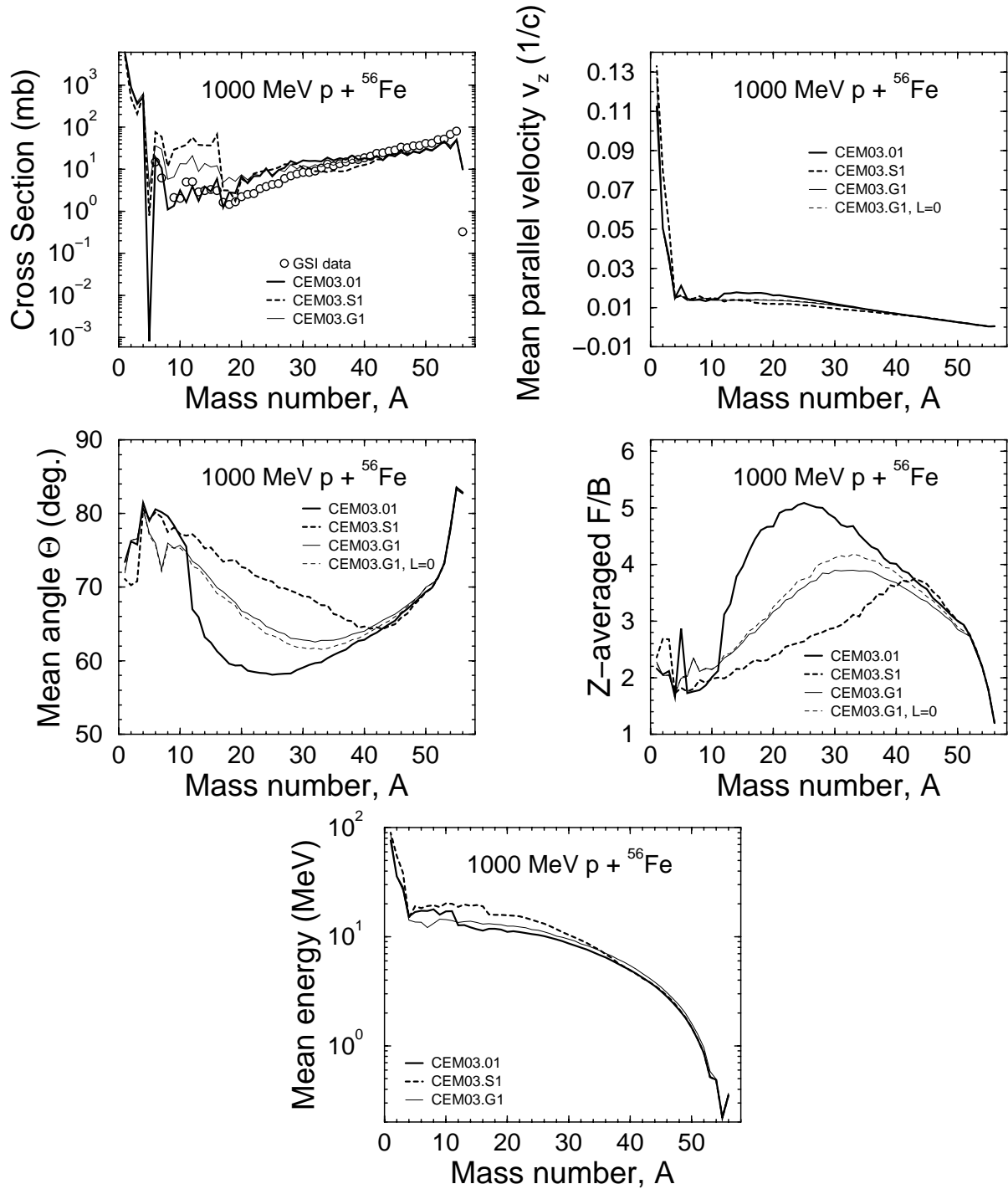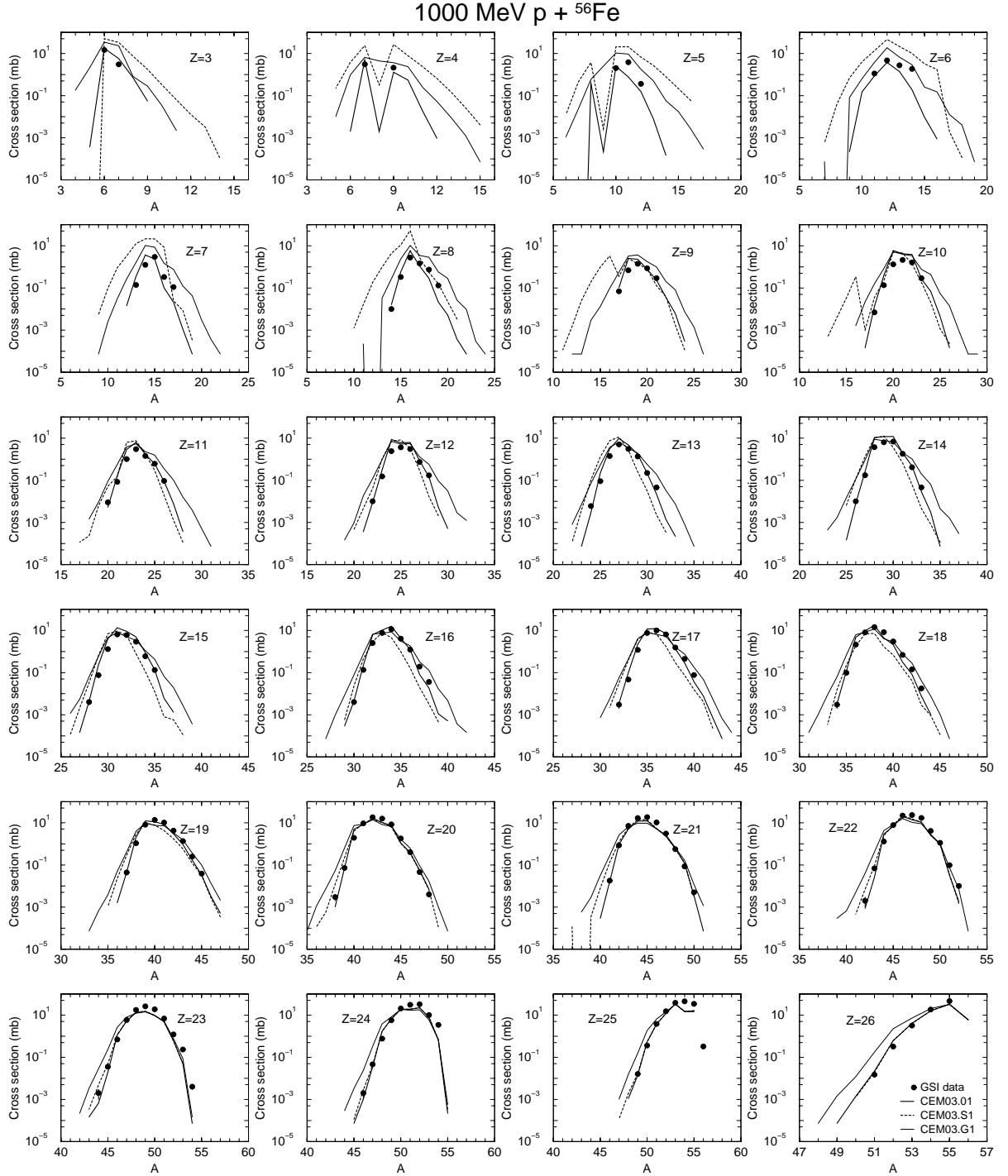
Figure 5: The same as in Fig. 2, but for the reaction 1000 MeV p + ^{56}Fe measured at GSI in inverse kinematics by Villagrasa (medium and heavy products) [37,38] and by Napolitani (light fragments) [39,40] with coauthors. To reveal the effect of angular momentum, L, of the compound nucleus on results calculated by GEMINI in CEM03.G1, the dashed thin lines show results obtained assuming $L = 0$ in GEMINI, that should be compared with the results shown by thin solid lines obtained with real values of L.

Figure 6: The same as in Fig. 3, but for the reaction 1000 MeV p + ^{56}Fe measured at GSI in inverse kinematics by Villagrasa (medium and heavy products) [37,38] and by Napolitani (light fragments) [39,40] with coauthors.
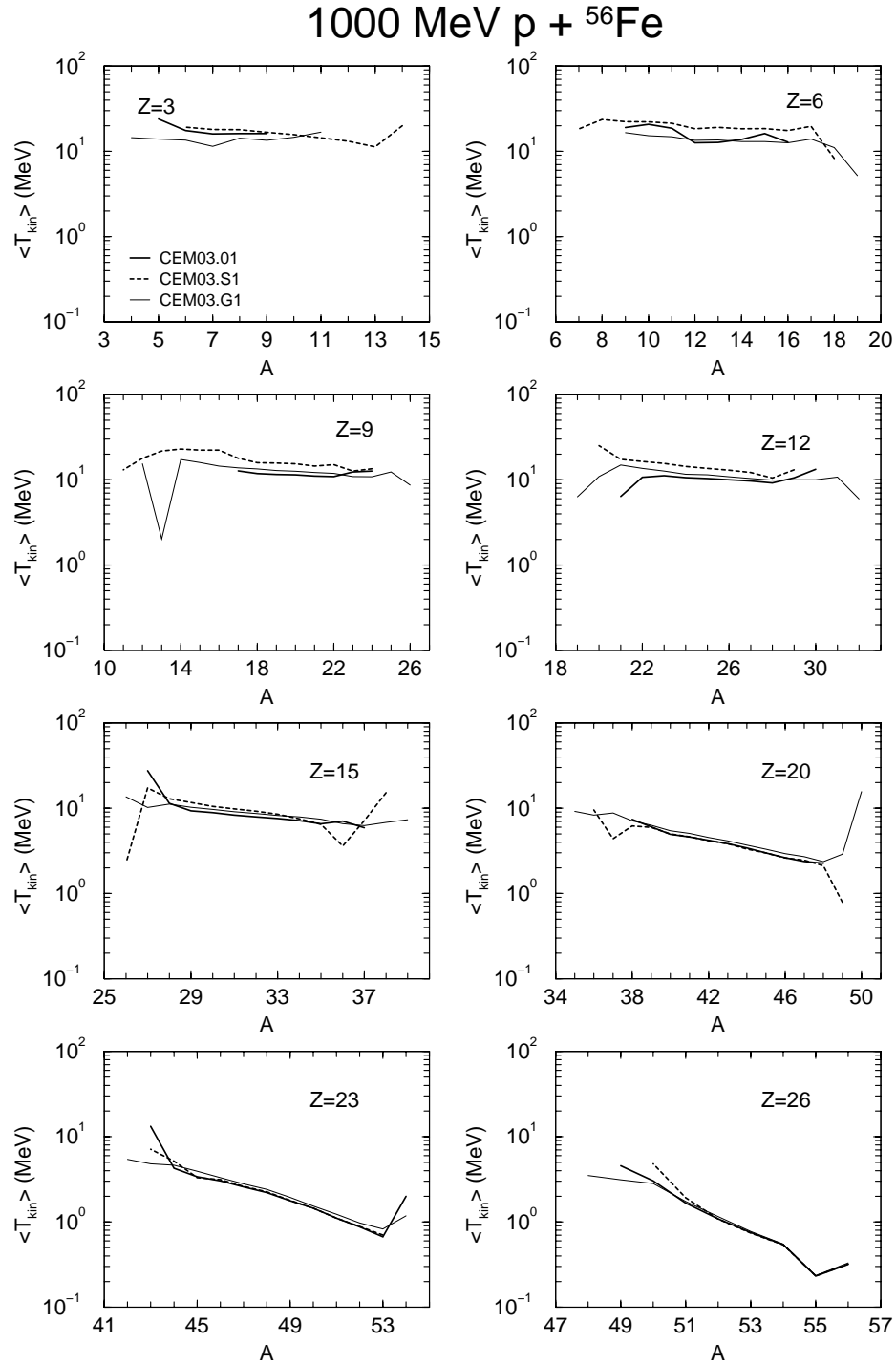
1000 MeV p + ^{56}Fe

Figure 7: The same as in Fig. 4, but for the reaction 1000 MeV p + ^{56}Fe.

used to study the effect of angular momentum in nuclear reactions. To reveal the effect of angular momentum, L, of the compound nucleus on the "recoil characteristics" $< \Theta >$, $< R >$, and $< v_z >$ of the reaction studied here, we have performed additional calculations with the "G" version of our codes assuming angular momentum of all compound nuclei being equal to zero. Results of such a modification of CEM03.G1 are shown in Fig. 5 with thin dashed lines, to be compared with the solid thin lines showing results by CEM03.G1 considering the real angular momenta of all compound nuclei. We see that the effect of angular momentum, L, of the compound nucleus on results for $< \Theta >$, $< R >$, and $< v_z >$ calculated by GEMINI in CEM03.G1 is more important for products with $12 < A < 46$, but is not very strong, on the whole.

Finally, Fig. 8 shows an example of proton-induced reactions at a higher energy and a heavier target, namely, 3.65 GeV p + ^{112}Sn, measured recently at JINR, Dubna with the activation technique [41]. We note that the CEM03.01, CEM03.S1, and CEM03.G1 results shown in the figure report A-distributions of the yield of all products, *i.e.*, sums over Z of yields of all isotopes with a given mass number A, while the experimental data obtained by the activation method generally represent results for only several isotopes (sometimes, for only a single isotope) that contribute to the corresponding data point. That is, this comparison is only qualitative but not quantitative and provides us only an approximate picture of the agreement between the calculations and measured data (just as we had in Fig. 1, where the data were also measured by the activation techniques at JINR). Activation measurements present the total yield for a given A only for cases when cumulative cross sections that include contributions from all precursors of all possible Z to the given measured yield; therefore, in general theoretical calculations of A-distribution of yields should be higher than many experimental activation data points. A much better, quantitative analysis would be to compare only the measured cross sections, isotope-by-isotope. Such a comparison of the measured data with results by CEM03.01 and LAQGSM03.01 (and by FLUKA and LAHET) is made in the original publication [41] and is not an aim of the present work. As the energy of the reaction shown in Fig. 8 is much higher than of all other reactions shown in previous figures, the situation is also quite different. We see that the standard CEM03.01 predicts production of isotopes with all possible mass numbers, from 1 to 112. Intermediate isotopes with mass numbers $28 < A < 80$ are produced by CEM03.01 only via deep spallation, *i.e.*, the INC, followed by preequilibrium emission of particles up to ^{4}He, followed by evaporation of particles and light fragments up to $A < 28$ from excited compound nuclei, without considering multifragmentation or/and binary decays. The "S" version considers production of such isotopes also via multifragmentation, while the "G" version, via binary decays. Nevertheless, the yield of products with $28 < A < 80$ predicted by the standard CEM03.01 model is higher than the ones predicted by both the "S" and "G" versions. Only for products with $5 < A < 28$ do the "S" and "G" versions predict a much higher yield than CEM03.01 does. For fragments with $8 \leq A \leq 16$, the "G" version predicts a yield about a factor of five higher than the standard CEM03.01, while the "S" version predicts even a higher yield, almost two orders of magnitude more than CEM03.01 does. Unfortunately, no experimental data for such products from this reaction are available at present, so the question about the "real" mechanisms for the production of such isotopes and their yields remains open.
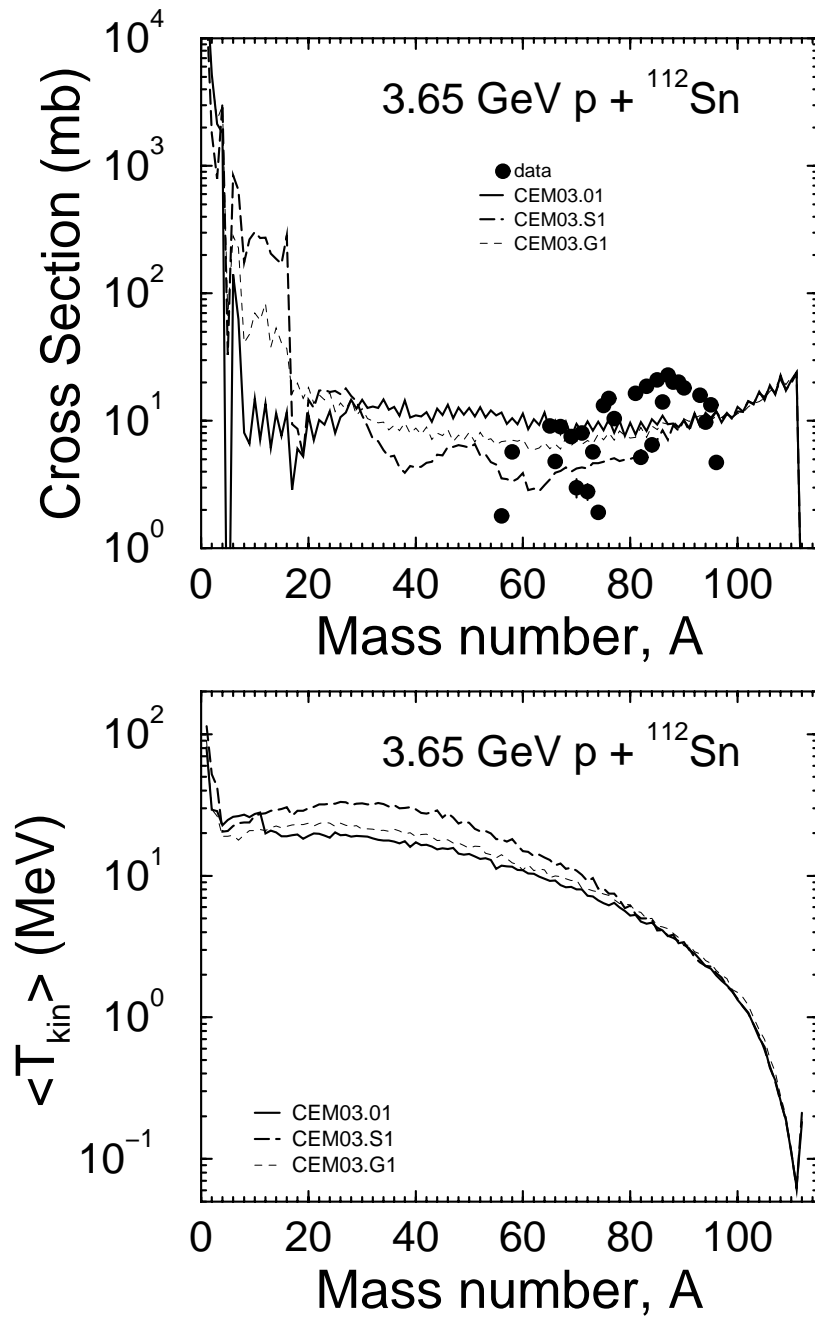
Figure 8: Predictions by CEM03.01, CEM03.S1, and CEM03.G1 for the mass number distribution of the product yield and the mean kinetic energy of all products in the laboratory system for the reaction 3.65 GeV p + ^{112}Sn (lines) compared with available experimental data (circles) [41], as indicated.

Fig. 9 shows one example of proton spectra from 500 MeV p + ^{58}Ni calculated with our CEM03.01, CEM03.S1, and CEM03.G1 codes compared with experimental data by Roy *et al.* [42]. As one may expect in advance, all three versions of our codes provide very similar results, in a good agreement with the measurement. The spectra by "S" and "G" versions are a little lower in the energy range $T_p \simeq 25$–50 MeV in comparison with the standard version CEM03.01, but the difference is less than a factor of two, and there are no experimental data for this part of spectra, so again it is difficult to conclude which version works better here.
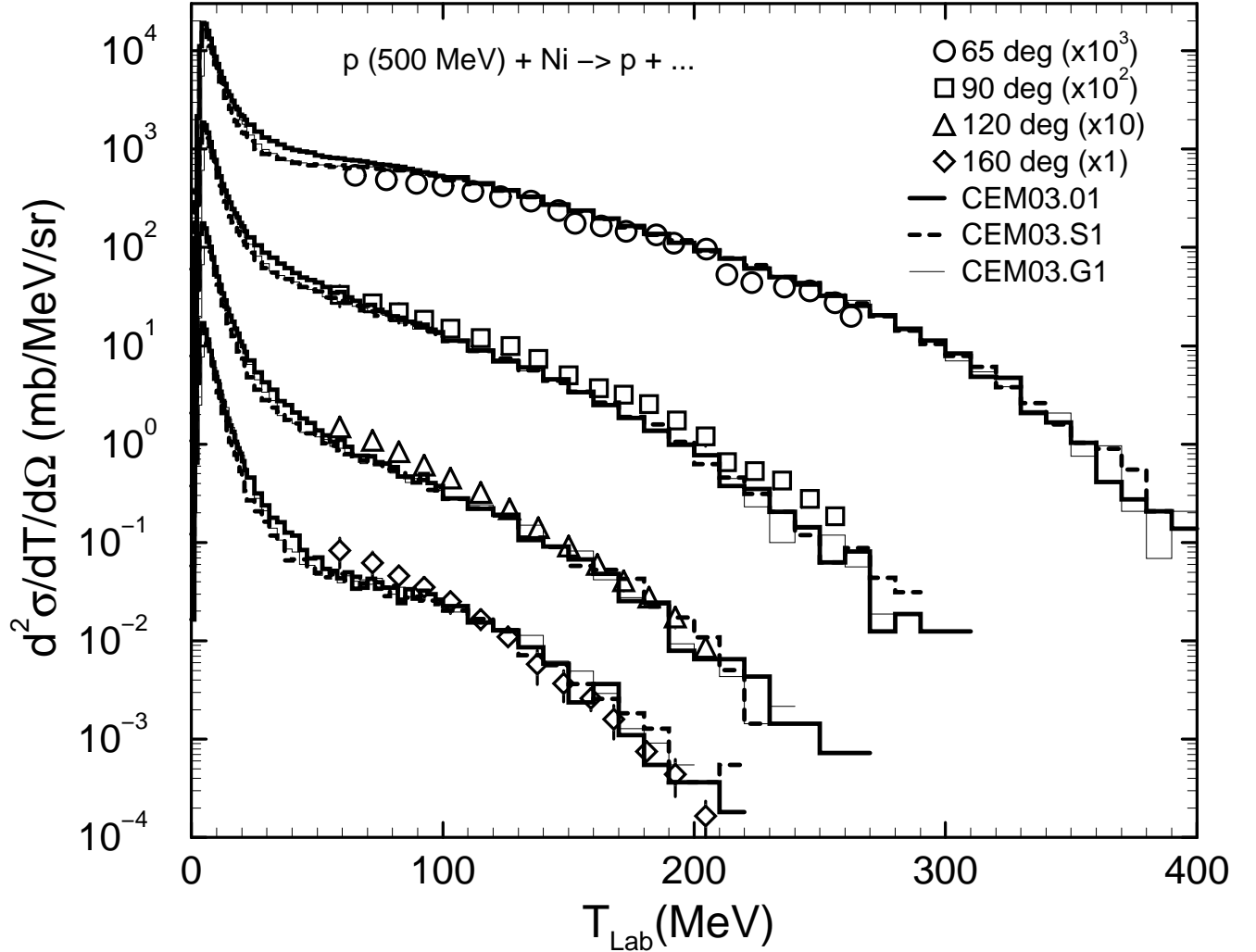
Figure 9: Experimental proton spectra from 500 MeV p + Ni [42] compared with CEM03.01, CEM03.S1, and CEM03.G1 results, as indicated.

The next two figures, Figs. 10 and 11, compare results by CEM03.01, CEM03.S1, and CEM03.G1 for the total production cross sections of H, He, Li, and Be isotopes produced in interactions of 1.2 GeV protons with thirteen target-nuclei from Al to Th, measured just recently at the Cooler Synchrotron Facility COSY of the Forschungszentrum Jülich [43].
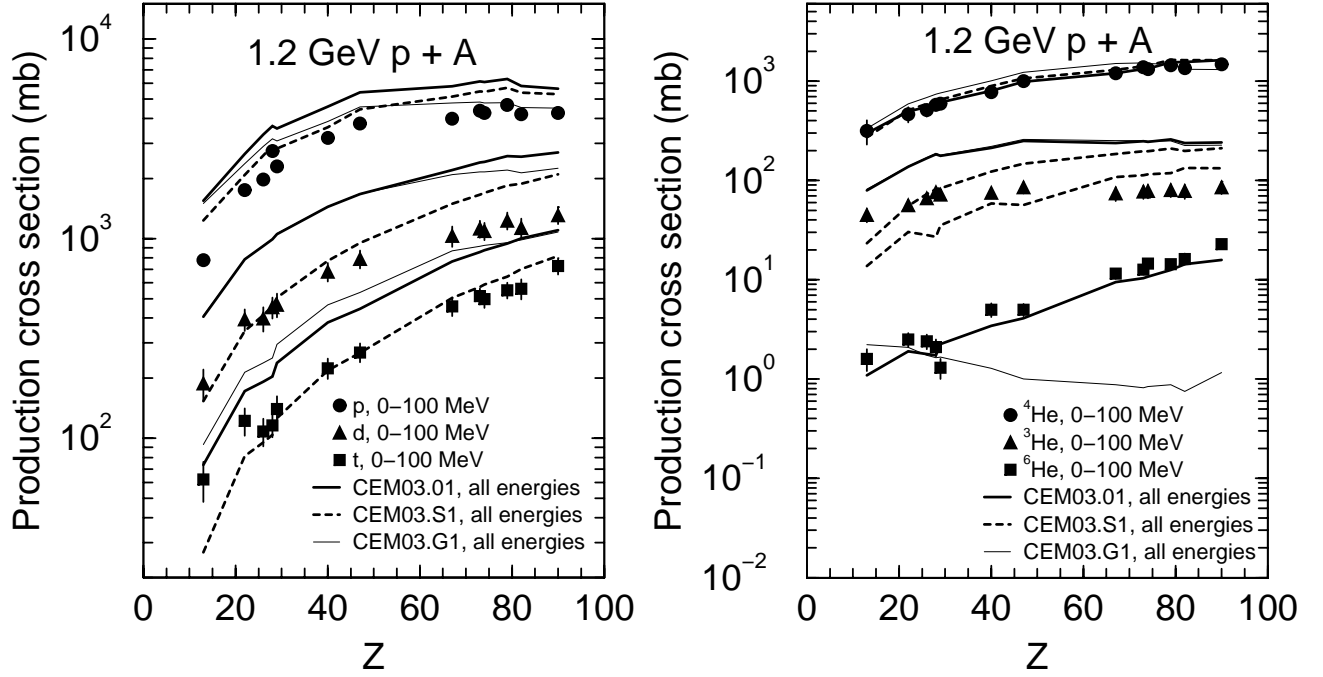
Figure 10: Comparison of measured [43] (symbols) production cross sections of hydrogen and helium isotopes with kinetic energies below 100 MeV for 1.2 GeV proton-induced reactions on targets between Al and Th with results by CEM03.01, CEM03.S1, and CEM03.G1 (lines), as indicated. Calculated results include contribution from products of all possible energies. An estimate of contributions from high-energy ($T > 100$ MeV) tails of calculated spectra to (not measured) production yields is shown in Fig. 12: It is of only about 17% for p, 3% for d, 1% for t, 2% for He3, and 0.4% for He4, in the case of Ag, using CEM03.01.

We note that the experimental data shown in Figs. 10 and 11 were taken from Tables 4, 5, and 6 of Ref. [43] and present the measured production cross sections of H, He, Li, and Be isotopes with kinetic energies of only below 100 MeV. We did not modify all versions of our codes to account for this experimental upper limit of the energy of detected particles; instead, we did an estimation of the contributions from the high-energy tails ($T > 100$ MeV) of calculated spectra to the total calculated production cross sections. Fig. 12 shows an example of our estimation, on angle-integrated energy spectra of p, d, t, ^{3}He, and ^{4}He calculated by CEM03.01 for the reaction 1.2 GeV p + Ag. The legend of this figure presents integrals of spectra (in mb) over the energy for particle energies above and below 100 MeV, respectively, and the percentage of contribution from high-energy tails ($T > 100$ MeV) of spectra to the total calculated cross sections. We see that for this particular reaction these contributions are rather small, of only about 17% for p, 3% for d, 1% for t, 2% for ^{3}He, and 0.4% for ^{4}He. Of course, for other targets and versions of our codes, these contributions are different, but on the whole they remain small, of only several percents. This is why we can compare in Figs. 10 and 11 our total production cross sections calculated for all energies with experimental data that include energies only below 100 MeV.
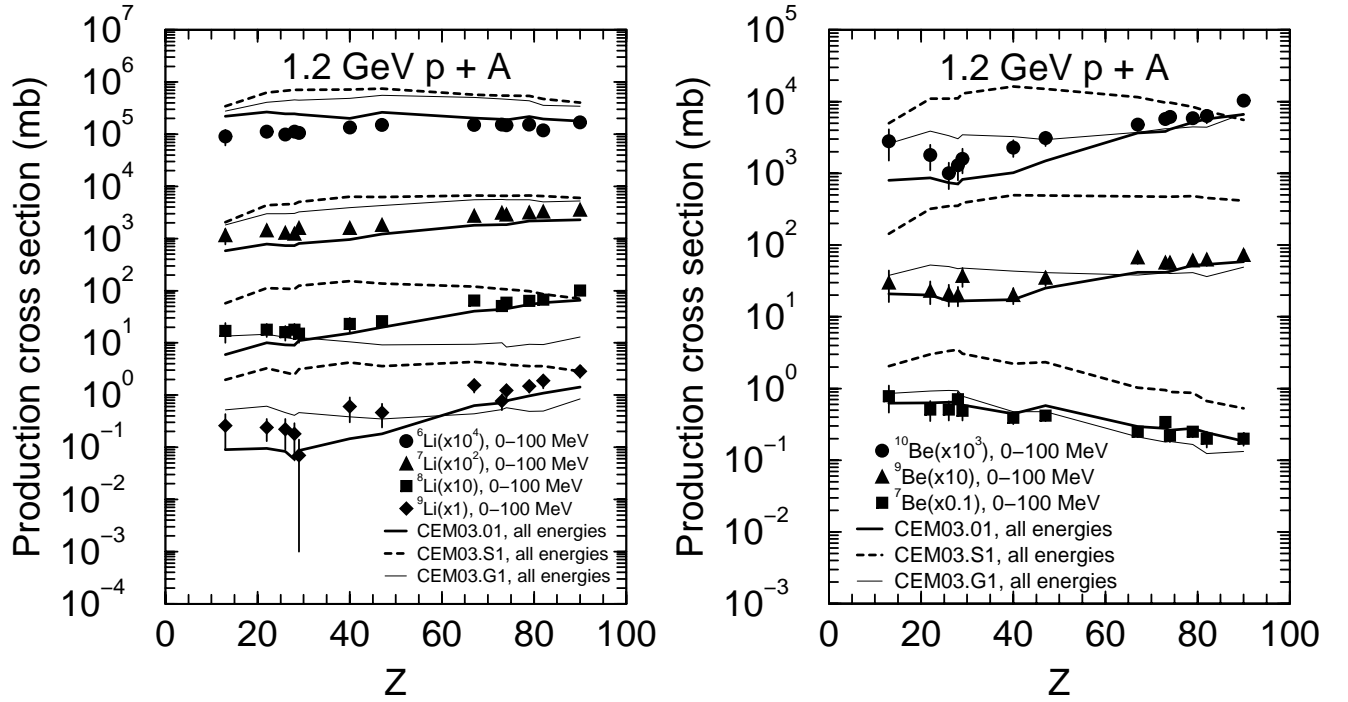
Figure 11: The same as in Fig. 10, but for the production of Li and Be isotopes.

We see that on the whole, with only a few exceptions, all versions of our codes describe reasonably the shape and the absolute values of the measured total production cross sections for all particles, from protons to ^{10}Be. The "S" version overestimates up to several times the yields of all Li isotopes and of ^{10}Be from light and medium nuclei, the yields of ^{7}Be and ^{9}Be from all targets, and up to an order of magnitude the yields of ^{6}He from all targets. On the other hand, it agrees better than other versions of our codes with the data for all H as well as for ^{3}He and ^{4}He isotopes. The "G" version predicts reasonably well the yields of all H, all Be, ^{3}He, ^{4}He, ^{6}Li, ^{7}Li, and not so well for ^{9}Li isotopes, but the shape of the calculated lines for the yields of ^{8}Li, and especially of ^{6}He, disagrees with the data. On the whole, a better agreement with all measured data is observed for the standard version of our code, CEM03.01.

At this point, we switch to analysis of several heavy-ion induced reactions with different versions of LAQGSM (CEM does not describe reactions induced by nuclei). Figs. 13 and 14 show a comparison of LAQGSM03.01, LAQGSM03.S1, and LAQGSM03.G1 results for the total production cross sections (yields) of nuclides with Z from 10 to 55 (all measured isotopes) produced from the fragmentation of ^{124}Xe in 1 GeV/A ^{124}Xe + ^{208}Pb collisions with the very recent GSI measurements [44]. Fig. 15 shows predictions by our models for the mass number distribution of the product yield and the mean kinetic energy (in the projectile frame of reference) of all products from the same reaction compared with available data [44].
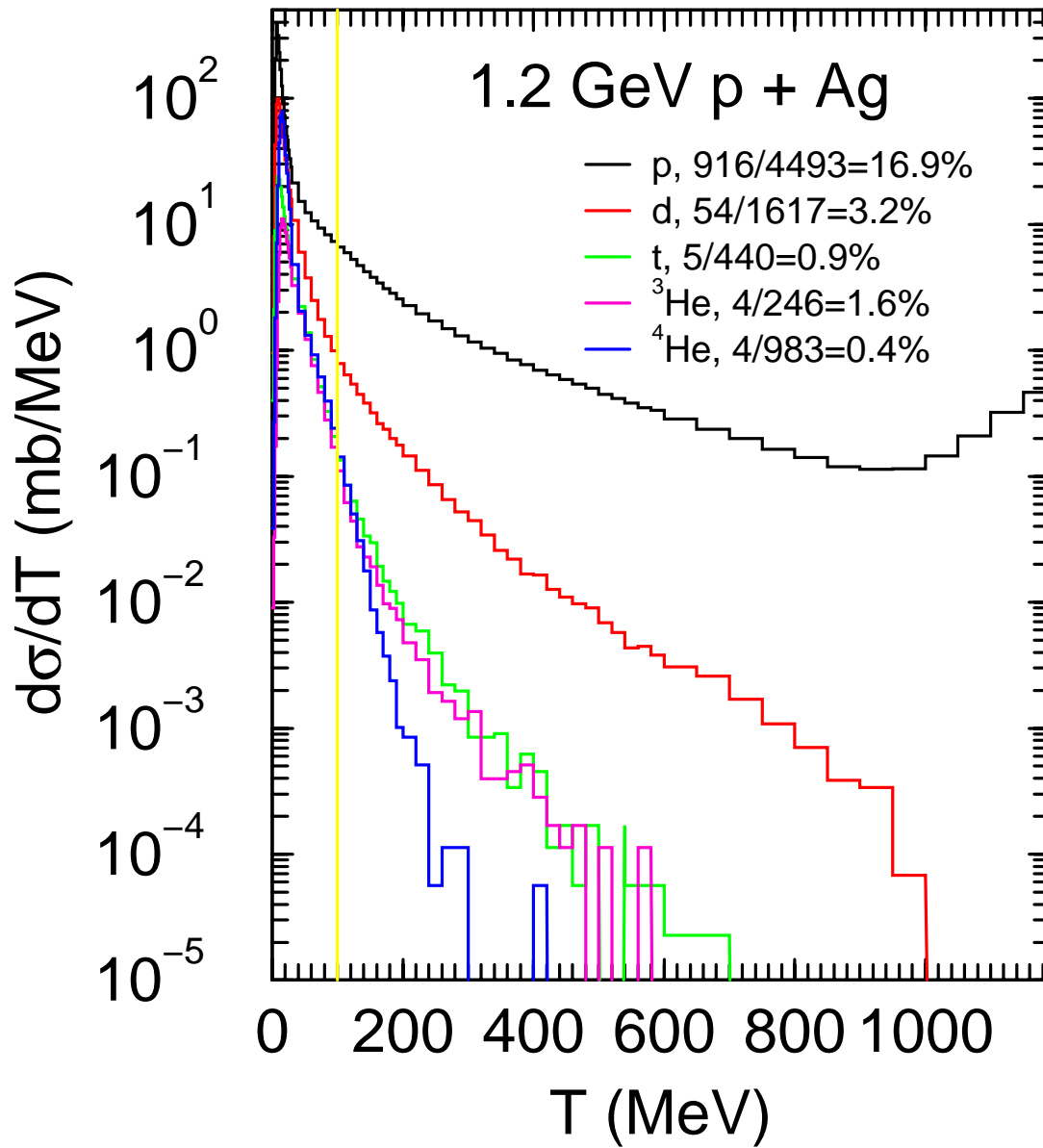
Figure 12: Angle-integrated energy spectra of p, d, t, ^{3}He, and ^{4}He emitted from the reaction 1.2 GeV p + Ag, as predicted by CEM03.01. The legend provides integrated production cross sections (in mb) for particles with energies above and below 100 MeV, respectively. These integrated cross sections are used to estimate the contributions from high energy ($T > 100$ MeV) tails of calculated spectra to the total calculated production yields: These contributions are of only about 17% for p, 3% for d, 1% for t, 2% for ^{3}He, and 0.4% for ^{4}He, in the case of Ag and results by CEM03.01.
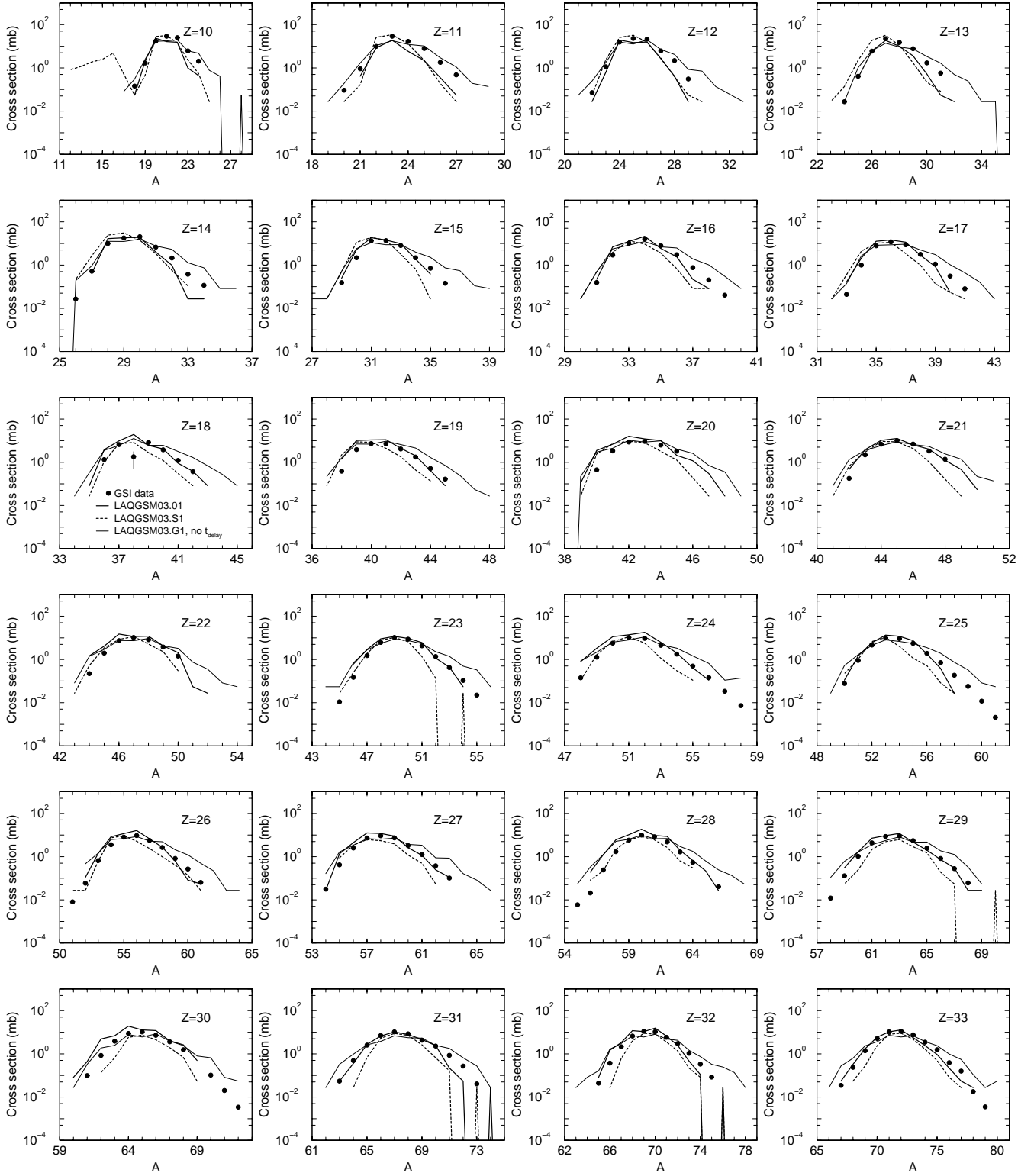
1 GeV/A ^{124}Xe + ^{208}Pb

Figure 13: Comparison of LAQGSM03.01, LAQGSM03.S1, and LAQGSM03.G1 results (lines) for the total cross sections (yields) of nuclides with Z from 10 to 33 produced from fragmentation of ^{124}Xe in 1 GeV/A ^{124}Xe + ^{208}Pb collisions with the recent GSI measurements [44] (circles), as indicated. No delay time in GEMINI is considered in the LAQGSM03.G1 calculation of this reaction.
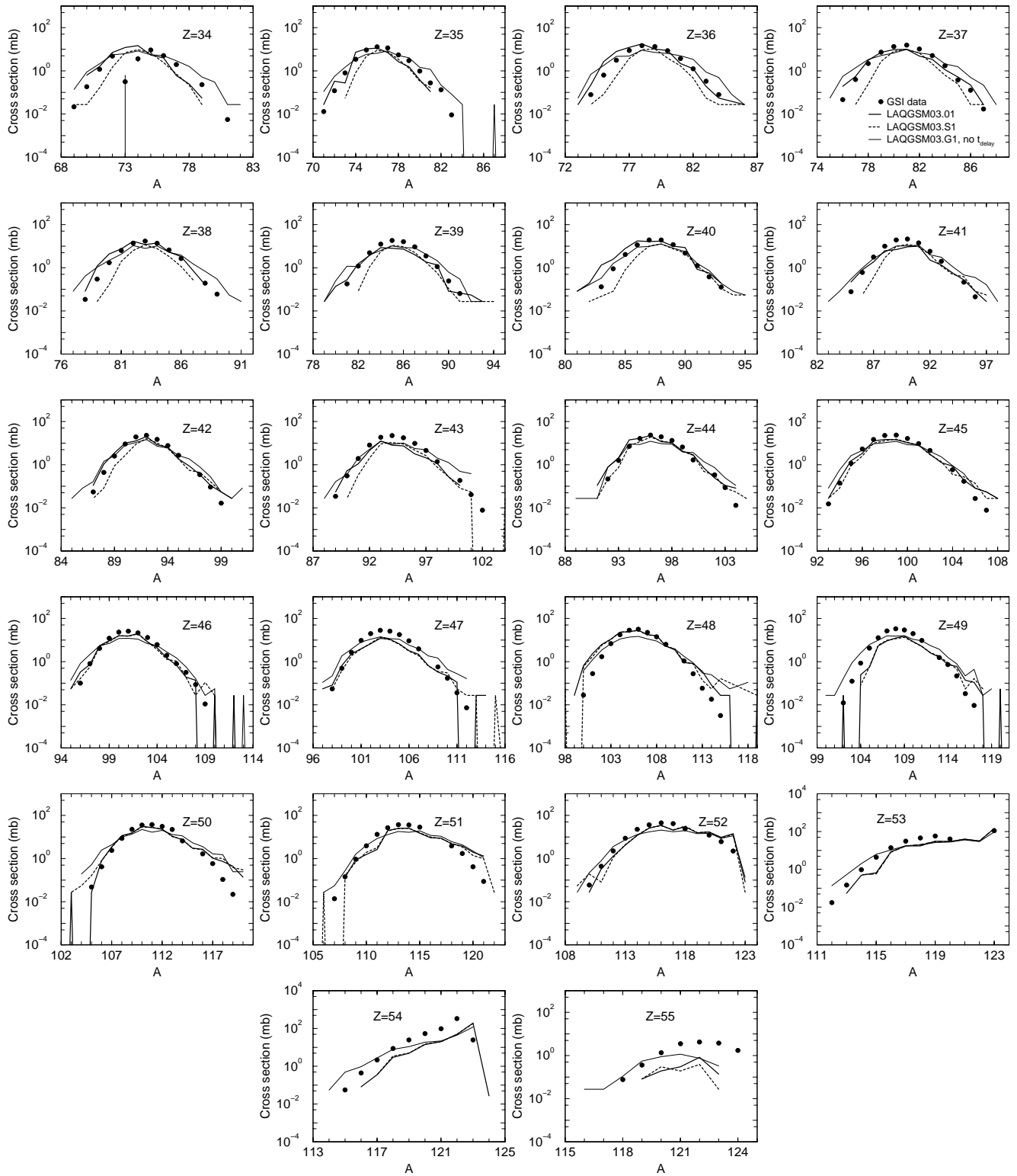
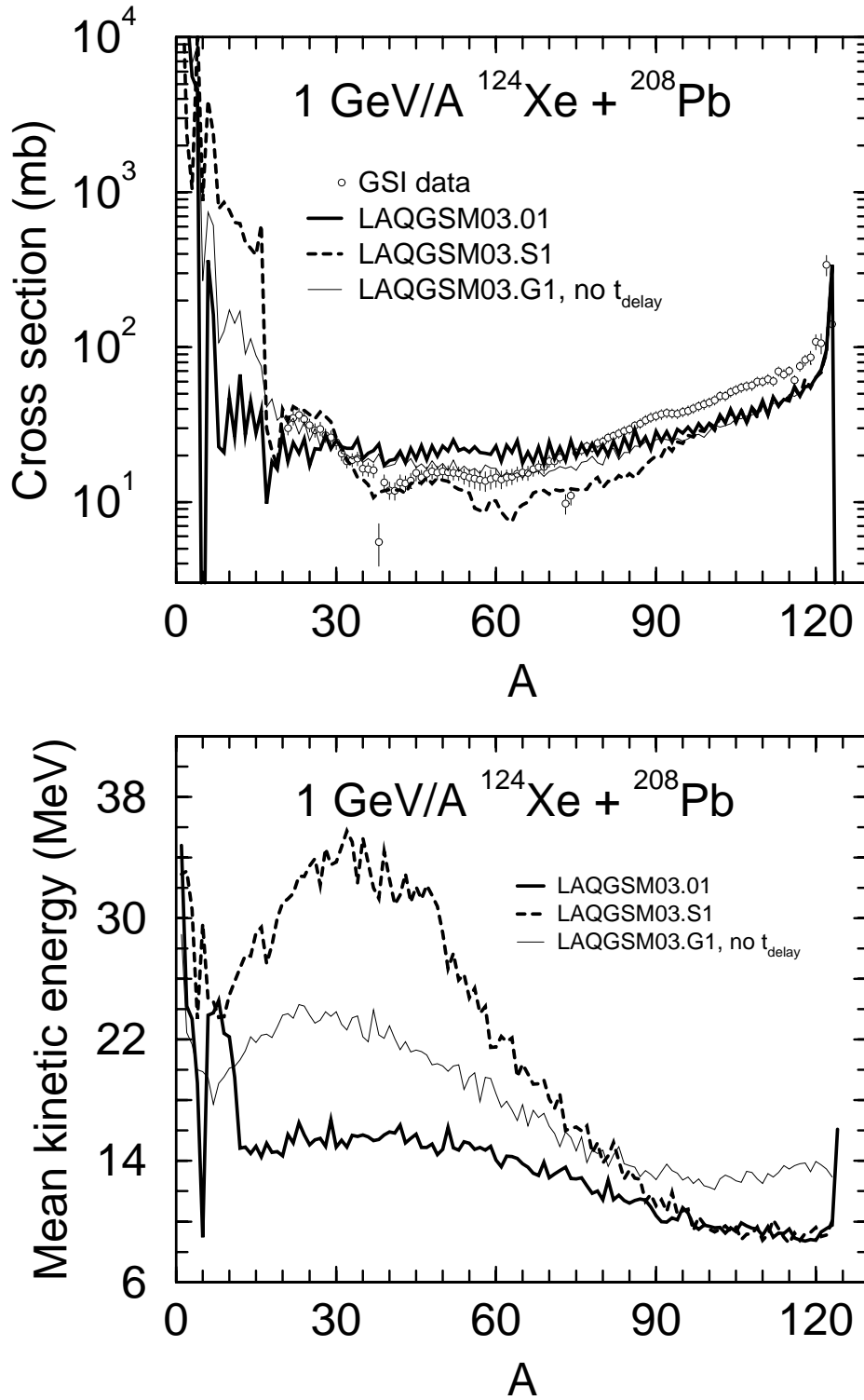Figure 14: The same as in Fig. 13, but for products with Z from 34 to 55.

Figure 15: Predictions of LAQGSM03.01, LAQGSM03.S1, and LAQGSM03.G1 for the mass number distribution of the product yield and the mean kinetic energy of all products from the fragmentation of ^{124}Xe (in the beam system) from the 1 GeV/A ^{124}Xe + ^{208}Pb reaction (lines) compared with available experimental data (circles) [44], as indicated.

We see that all versions of our codes describe reasonably well cross sections for the production of all measured isotopes, from Neon to Cesium. A prediction by LAQGSM03.S1 of several unstable Neon isotopes with mass numbers lower than 18 not measured in the experiment (upper-left plot in Fig. 13) does not bother us much: These unstable isotopes should be disintegrated into stable nuclei. The transport codes using our event generators do take care of this; we could also add a checking of such unstable products into our codes and disintegrate them with our event generators before transferring their results to transport codes.

As observed above for proton-induced reactions, the standard version LAQGSM03.01 describes the production cross sections of all isotopes from 1 GeV/A ^{124}Xe + Pb on the whole a little better than the "S" and/or "G" versions do. We believe that the reason for this is the same as we had for proton-induced reaction: LAQGSM03.01 was developed carefully during the last several years; the nuclear reaction models considered by it were adjusted to each other and their parameters were fitted to describe as well as possible arbitrary reactions. The "S" and "G" versions of LAQGSM03.01 were developed here without any additional fitting or adjustment of any parameters. We think, it would be possible to adjust the models of the "G" and "S" versions and to fit their parameters so that they describe production cross sections no worse than the standard version does, but this was outside the aim of the present work.

From comparison of only the measured [44] product yields with calculations by different versions of LAQGSM it is difficult, if not impossible, the uncover the "real" mechanisms of nuclear reactions contributing to the production of measured isotopes. In the upper plot of Fig. 15, we see a big difference between predictions by the standard, "S", and "G" versions for the yields of isotopes with $15 < A < 31$, up to an order of magnitude and higher, but, unfortunately, these products were not measured [44]. We see also quite a big difference between the predictions by different versions for the mean kinetic energy of products with $20 < A < 80$ (lower plot in Fig. 15), but we do not have experimental data for this "recoil characteristics" either.

Figs. 16 and 17 show results very similar to the ones presented in Figs. 13 and 14, only for another reaction (projectile) measured lately at GSI, 1 GeV/A ^{136}Xe + Pb [44] (we made all calculations on mono-isotopic ^{208}Pb targets but not on Lead with a natural composition of isotopes as was measured, just as we did for the results presented in Figs. 13–15). The situation for this reaction is very similar to the one induced by ^{124}Xe shown in Figs. 13 and 14. All comments made above for the ^{124}Xe projectiles (Figs. 13 and 14) are valid and could be repeated here again for reactions induced by ^{136}Xe (Figs. 16 and 17). Let us note that ^{124}Xe is the most neutron-deficient stable isotope of Xenon, while ^{136}Xe is the most neutron-rich one; this indicates us that our event generators describe equally well reactions involving both neutron-deficient and neutron-rich nuclei.

The only difference between results shown in Figs. 16 and 17 for ^{136}Xe in comparison with results for ^{124}Xe shown in Figs. 13 and 14 is that for ^{136}Xe we performed two sets of calculations with the "G" version of LAQGSM: without taking into account the delay time (results shown with thin solid lines) and with values $t_{delay} = 75$ and $\sigma_{delay} = 50$ (results shown with thin dashed

lines) for the time delay parameters of GEMINI (see Section 3.G above). The reason for this additional study we performed for reactions induced by ^{136}Xe is to understand how results by LAQGSM03.G1 depend on the value of the time delay parameters of GEMINI: These parameters of GEMINI are considered as input parameters of the model and it is up to users to chose them. For instance, for proton-induced reactions, we found [45] that: 1) GEMINI merged with CEM/LAQGSM provides reasonably good results for medium-heavy targets without a fission delay time; 2) For preactinides, we have to use $t_{delay} = 50$–70 and $\sigma_{delay} = 1$–50, otherwise GEMINI provides too much fission — this may be related to the calculation of fission barriers of preactinides with strong ground-state shell corrections in the version of GEMINI we use; 3) The current version of GEMINI does not work well for actinides.

Our results shown on Figs. 16 and 17 (and on the left panels of Figs. 18 and 19) are only for products of fragmentation of the projectile, ^{136}Xe, just as reactions are measured at GSI [44]. For such processes, we do not see a big difference between results by LAQGSM03.G1 obtained without taking into account the delay time (thin solid lines) and the ones calculated with $t_{delay} = 75$ and $\sigma_{delay} = 50$ (thin dashed lines). This is similar to what we found for proton-induced reactions [45]: As ^{136}Xe is a medium-heavy target, it can be calculated with GEMINI without taking into account the delay time. The situation changes dramatically if we look in the laboratory system at all products from this reaction, just as happens in nature, produced from both the projectile ^{136}Xe and the target ^{208}Pb (see the right panels on Figs. 18 and 19). ^{208}Pb is a preactinide nucleus and has to be calculated with GEMINI using $t_{delay} = 75$ and $\sigma_{delay} = 50$, according to our experience gained form studying proton-induced reactions [45] (this is why we chose here these values of t_{delay} and σ_{delay}). From the results presented on plots in the right panels of Figs. 18 and 19, we see that all characteristics of isotopes produced from the target ^{208}Pb calculated with $t_{delay} = 75$ and $\sigma_{delay} = 50$ differ significantly from the ones calculated without taking into account the delay time in GEMINI. Unfortunately, these characteristics can not be measured with the GSI technique, and we have no experimental data with which to compare our results.

Just as observed above for reactions induced by ^{124}Xe and protons, from comparison of only the measured [44] product yields from reactions induced by ^{136}Xe (Figs. 16 and 17) with calculations by different versions of LAQGSM it is difficult, if not impossible, to reveal the "real" mechanisms of nuclear reactions contributing to the production of measured isotopes. This is why for reactions induced by ^{136}Xe, we look additionally at several "recoil characteristics" like $< T_{kin} >$, $< v_z >$, $< \Theta >$, and $< R >$, as we did above for proton-induced reactions (Figs. 1, 2, and 5). The left panels of plots in Figs. 18 and 19 show such characteristics (plus, the Z-integrated mass product yield and the cross section for the production of nuclides with $Z = 56$, shown in Fig. 18) calculated in the projectile frame of reference, as all reactions at GSI are measured [44]. We see a big difference between results of the standard version of LAQGSM and of its "G" and "S" versions for the calculated Z-integrated yield of isotopes with $15 < A < 31$, for $< T_{kin} >$ of isotopes with $20 < A < 80$, and for $< v_z >$, $< \Theta >$, and especially for $< R >$ of almost all products. Unfortunately, none of these characteristics were measured at GSI so we can not identify a specific reaction mechanism based on these results, until experimental data are available.
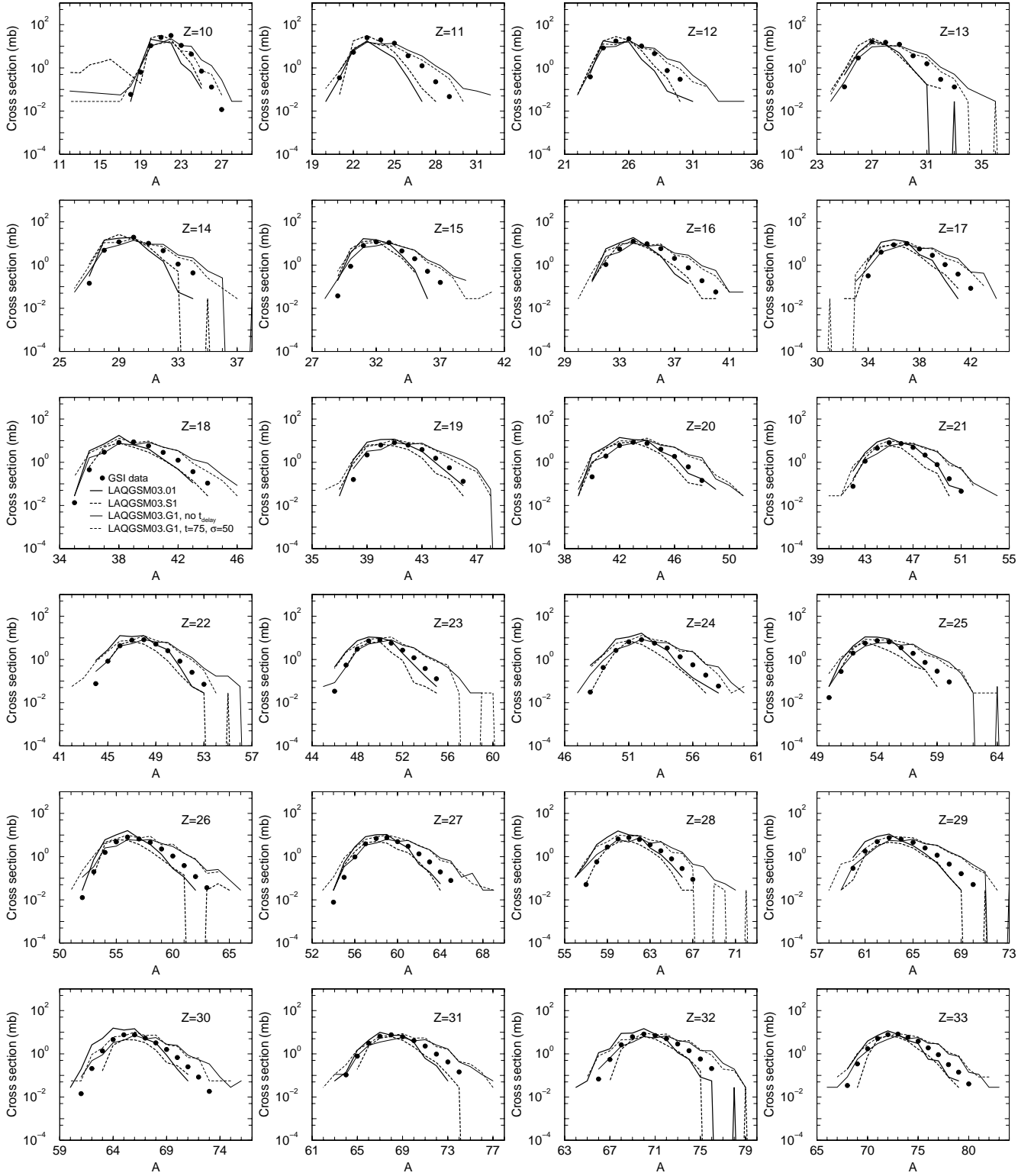
Figure 16: Comparison of LAQGSM03.01, LAQGSM03.S1, and LAQGSM03.G1 results (lines) for the total cross sections (yields) of nuclides with Z from 10 to 33 produced from fragmentation of ^{136}Xe in 1 GeV/A ^{136}Xe + ^{208}Pb collisions with the GSI data [44] (circles), as indicated. Results by LAQGSM03.G1 calculated without delay time in GEMINI and with $t_{delay} = 75$ and $\sigma_{delay} = 50$ are shown by solid and dashed thin lines, respectively.

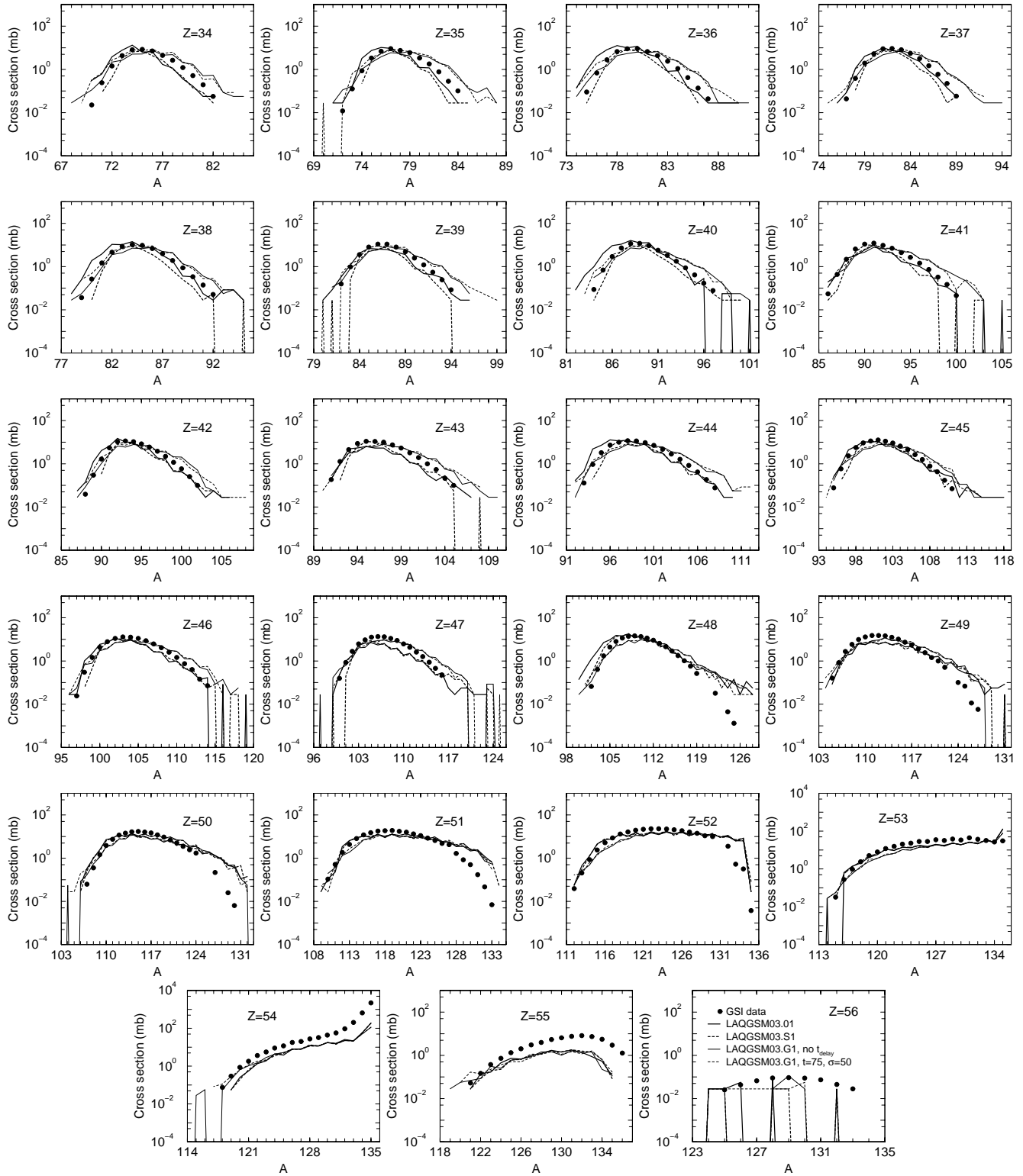1 GeV/A ^{136}Xe + ^{208}Pb

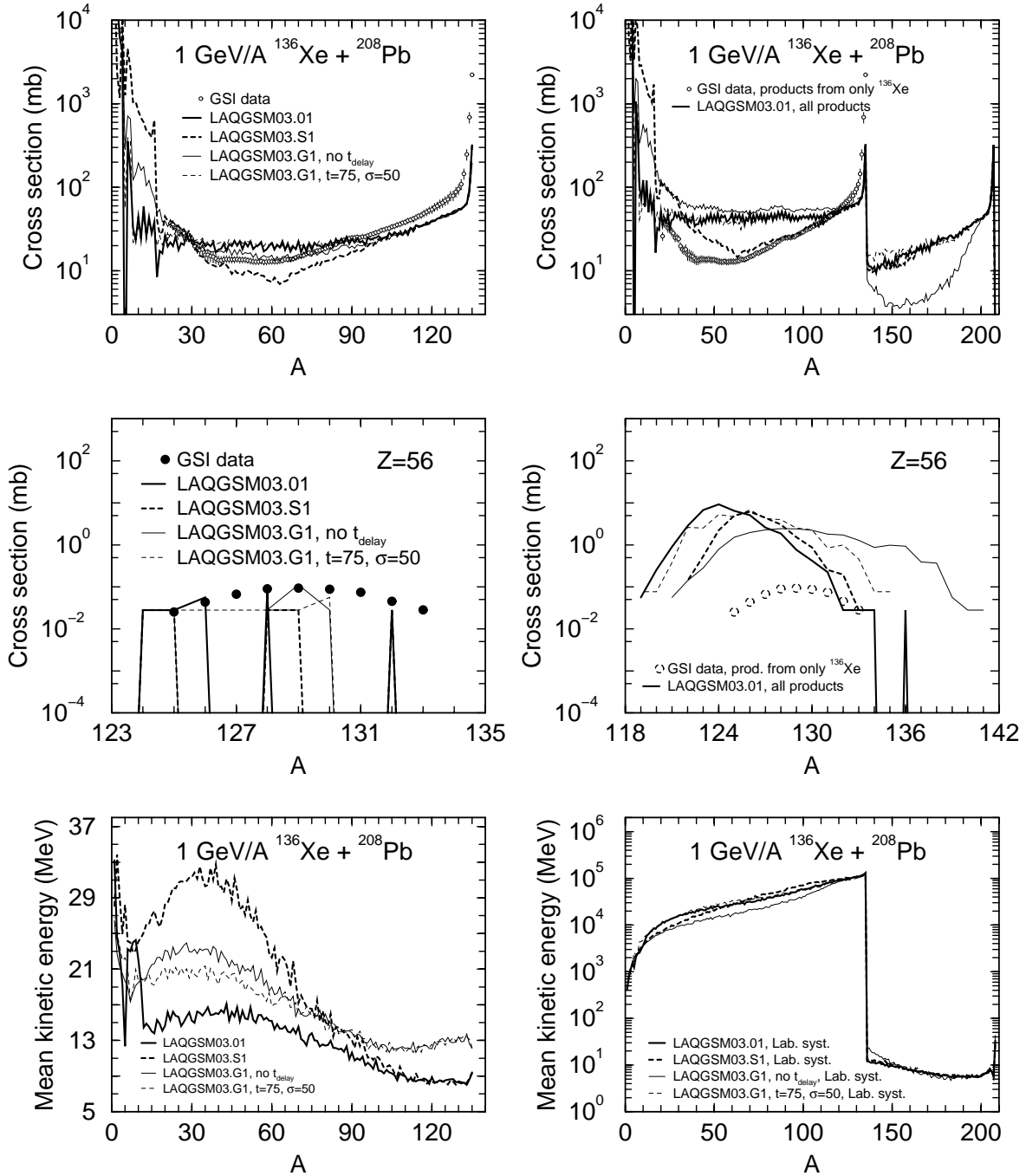Figure 17: The same as in Fig. 16, but for products with Z from 34 to 56.

Figure 18: **Left panel:** Predictions of LAQGSM03.01, LAQGSM03.S1, and LAQGSM03.G1 for the Z-integrated mass product yield, cross section of the production of nuclides with $Z = 56$, and the mean kinetic energy of all products from the fragmentation of ^{136}Xe (in the beam system) from the 1 GeV/A ^{136}Xe + ^{208}Pb reaction (lines) compared with available experimental data (circles) [44], as indicated. **Right panel:** The same as on the left panel, but calculated in the laboratory system, as "seen" by a transport code, for all nuclides produced from both the target, ^{136}Xe, and the projectile, ^{208}Pb. Experimental data (dashed circles on the right panel) are measured in the beam system and should be compared only with the results showed on the left panel; this is why they do not agree with the laboratory system results to be used by transport codes shown in the right panel.
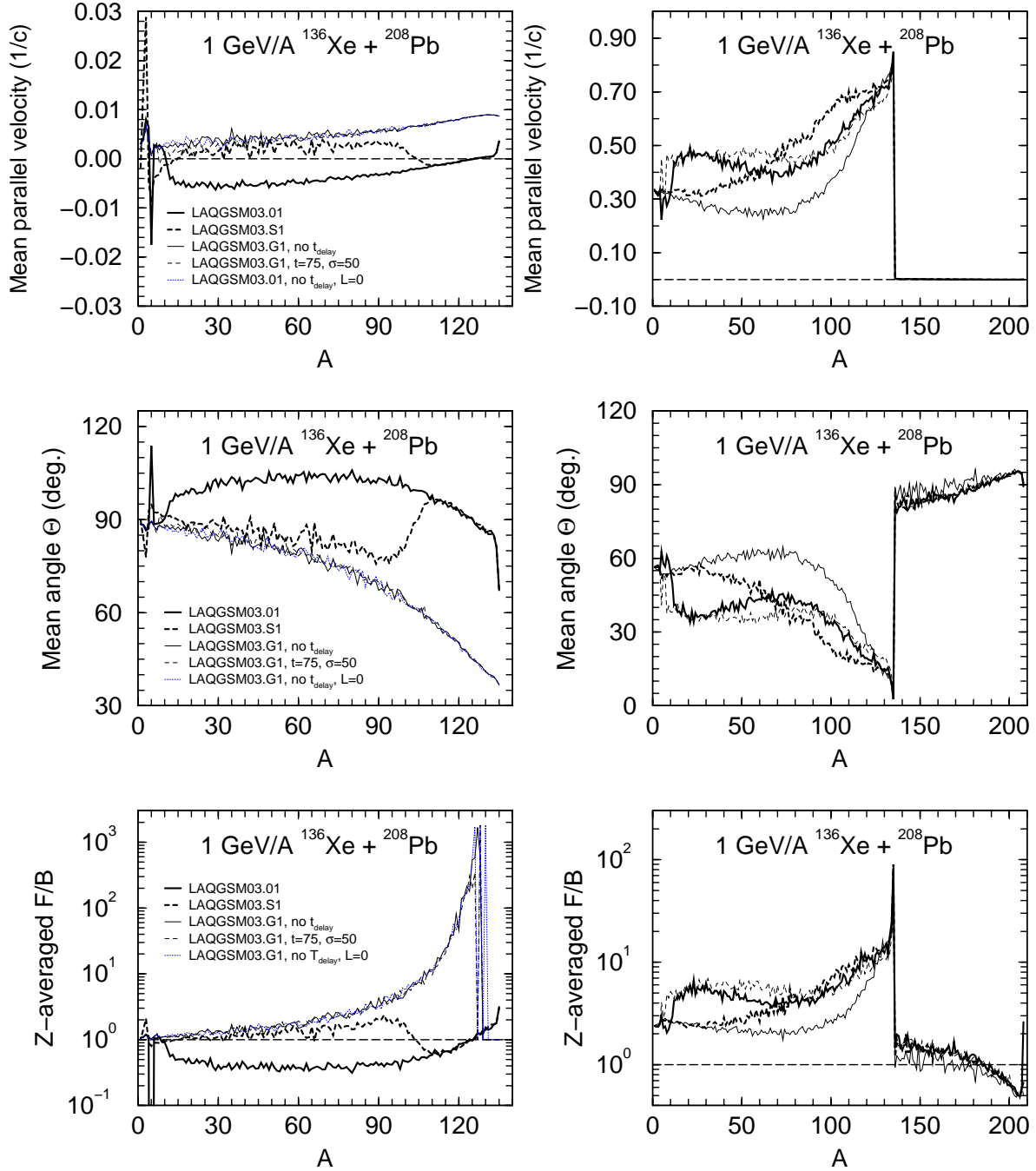
Figure 19: The same as in Fig. 18, but for the mean parallel velocity v_z, mean production angle Θ, Z-averaged A-dependence of the F/B ratio of the forward product cross sections to the backward ones. To reveal the effect of angular momentum, L, of the compound nucleus on results calculated by GEMINI in LAQGSM03.G1, the blue dotted thin lines on the left panel show results obtained assuming $L = 0$ in GEMINI, which should be compared with the results shown on the same plots by thin solid black lines obtained using actual values of L.

To reveal the effect of angular momentum, L, of the compound nucleus on the "recoil characteristics" $< v_z >$, $< \Theta >$, and $< R >$ of the reaction induced by ^{136}Xe, we have performed additional calculations with LAQGSM03.G1 assuming the angular momentum of all compound nuclei is equal to zero. Results of such a modification of LAQGSM03.G1 are shown in Fig. 19 with blue dotted thin lines, to be compared with the thin black solid lines showing results from LAQGSM03.G1 considering the real angular momenta of all compound nuclei (both of these calculations have no delay time in GEMINI). We see that the effect of angular momentum, L, of the compound nuclei on results for $< \Theta >$, $< R >$, and $< v_z >$ calculated by GEMINI in LAQGSM03.G1 is not significant.

Together with results for products from only fragmentation of the projectile calculated in the projectile frame of reference (as all measurements at GSI are done) shown on the left panels of Figs. 18 and 19, on the right panels of the same figures, we show side-by-side similar results calculated in the laboratory system that include isotopes produced from both the projectile and the target. This is the way a reaction really happens in nature, and how a transport code "sees" and uses it in transport calculations from results provided by event generators like LAQGSM. Unfortunately, none of the currently available experimental techniques allow the measurement of all products of heavy-ion reactions, produced from both the projectiles and targets. We can not yet compare the results shown on the right panels with any measurements. However, we find them quite interesting and informative for nuclear applications, including to users and developers of transport codes.

Several phenomenological systematics are presently available in the literature to estimate the cross sections of products from the fragmentation of the projectile in a heavy-ion reaction, with the most advanced and often used, especially at GSI, the EPAX parameterization by K. Sümmerer and B. Blank [46]. Such systematics are very fast and easy to calculate; they are useful and provide quite reliable results to estimate the fragmentation of the projectile in a heavy-ion reaction, especially if experimental data for that reaction, or for a not too different one, were used in deriving the phenomenological systematics. But phenomenological systematics may not provide reliable results for unmeasured reactions that differ significantly from those used in fitting its parameters. In addition, one should be very careful when using systematics like EPAX in applications; the point is that most applications need all products from a reaction, in the laboratory system, while EPAX provides results from only fragmentation of the projectile. So for the reaction ^{136}Xe + ^{208}Pb discussed here, we can not use EPAX to calculate the inverse reaction ^{208}Pb + ^{136}Xe adding the results with the ones obtained for the direct Xe+Pb reaction with a hope to obtain all products from this reaction in the laboratory system exactly as happens in reality and calculated by an event generator. The point is that we have products from a heavy-ion reaction not only from the fragmentation of the projectile but also from the target. Depending on the incident energy of the projectile and on the impact parameter of the colliding nuclei, we may have a significant contribution from intermediate systems produced via the "fusion" of a part of the projectile with a part of the target. Such processes are missed by EPAX, while event generators like our LAQGSM account for them. This is why we need reliable

event generators rather than phenomenological systematics in applications. We plan to address this subject in more details in a later paper.

Summary

CEM03.S1, CEM03.G1, LAQGSM03.S1, and LAQGSM03.G1 versions of our CEM03.01 and LAQGSM03.01 event generators have been developed, completed, verified, validated and benchmarked against a variety of measured reactions and results by other models, and stored as "frozen" on several X-3 and T-16 computers. These "G" and "S" versions of our codes are to be used as stand-alone codes or as event generators in working versions of transport codes such as MCNP6, MARS, and MCNPX, when we are interested in the production of light and medium fragments from nonfissioning targets. We may consider also making them available to the public via the Radiation Safety Information Computational Center (RSICC) at Oak Ridge in the future.

REFERENCES

[1] S. G. Mashnik, K. K. Gudima, R. E. Prael, and A. J. Sierk, "Analysis of the GSI A+p and A+A Spallation, Fission, and Fragmentation Measurements with the LANL CEM2k and LAQGSM Codes," *Proc. TRAMU@GSI*, GSI-Darmstadt, Germany, 2003, ISBN 3-00-012276-1, Eds: A. Kelic and K.-H. Schmidt, http://www-wnt.gsi.de/tramu/; E-print: nucl-th/0404018.

[2] S. G. Mashnik, K. K. Gudima, I. V. Moskalenko, R. E. Prael, and A. J. Sierk, "CEM2k and LAQGSM as Event Generators for Space-Radiation-Shielding and Cosmic-Ray-Propagation Applications," Advances in Space Research **34** (2004) 1288–1296.

[3] S. G. Mashnik, K. K. Gudima, A. J. Sierk, and R. E. Prael, "Improved Intranuclear Cascade Models for the Codes CEM2k and LAQGSM," Proc. Int. Conf. on Nuclear Data for Sci. & Techn. (ND2004), September 26 - October 1, 2004, Santa Fe, NM, USA, edited by R. C. Haight, M. B. Chadwick, T. Kawano, and P. Talou, (AIP Conference Proceedings, Volume 769, Melville, New York, 2005), pp. 1188–1192.

[4] S. G. Mashnik, M. I. Baznat, K. K. Gudima, A. J. Sierk, and R. E. Prael, "CEM03 and LAQGSM03: Extension of the CEM2k+GEM2 and LAQGSM Codes to Describe Photo-Nuclear Reactions at Intermediate Energies (30 MeV to 1.5 GeV)," Journal of Nuclear and Radiochemical Science **6** (2005) A1–A19.

[5] K. K. Gudima, S. G. Mashnik, and V. D. Toneev, "Cascade-Exciton Model of Nuclear Reactions," Nucl. Phys. A **401** (1983) 329–361.

[6] Konstantin K. Gudima, Stepan G. Mashnik, and Arnold J. Sierk, "User Manual for the code LAQGSM," LANL Report LA-UR-01-6804, Los Alamos (2001), http://lib-www.lanl.gov/la-pubs/00818645.pdf.

[7] S. G. Mashnik, K. K. Gudima, M. I. Baznat, A. J. Sierk, R. E. Prael, and N. V. Mokhov, "CEM03.01 and LAQGSM03.01 Versions of the Improved Cascade-Exciton Model (CEM) and Los Alamos Quark-Gluon String Model (LAQGSM) Codes," Research Note X-5-RN (U) 05-11; LANL Report LA-UR-05-2686, Los Alamos (2005).

[8] S. G. Mashnik, A. J. Sierk, K. K. Gudima, M. I. Baznat, "CEM03 and LAQGSM03—New Modeling Tools for Nuclear Applications," Proc. European Physical Society 19th Nuclear Physics Division Conference **New Trends in Nuclear Physics Applications and Technology (NPDC19)**, Pavia, Italy, September 5–9, 2005, LANL Report LA-UR-05-8130, Los Alamos (2005), E-print: nucl-th/0510070, Journal of Physics: Conference Series, in press.

[9] Stepan G. Mashnik, Konstantin K. Gudima, Arnold J. Sierk, Mircea I. Baznat, and Nikolai V. Mokhov, "CEM03.01 User Manual," LANL Report LA-UR-05-7321, Los Alamos (2005).

[10] J. P. Bondorf, A. S. Botvina, A. S. Iljinov, I. N. Mishustin, and K. Sneppen, "Statistical Multifragmentation of Nuclei," Phys. Rep. **257** (1995) 133–221.

[11] A. S. Botvina, A. S. Iljinov, I. N. Mishustin, J. P. Bondorf, R. Donangelo, and K. Snappen, "Statistical Simulation of the Break-up of Highly Excited Nuclei," Nucl Phys. A **475** (1987) 663–686.

[12] A. S. Botvina, K. K. Gudima, A. S. Iljinov, and I. N. Mishustin. "Multifragmentation of Highly-Excited Nuclei in Nucleus-Nucleus Collisions at Intermediate Energies," Yad. Fiz. **57** (1994) 667–674 [Phys. At. Nucl. **57** (1994) 628–635].

[13] A. S. Botvina, A. S. Iljinov, and I. N. Mishustin, "Multifragmentation Break-up of Nuclei by Intermediate-Energy Protons," Nucl. Phys. A **507** (1990) 649–674.

[14] A. S. Botvina, A. S. Iljinov, and I. N. Mishustin, "Multifragmentation of Nuclei at Excitation-Energies Approximately 10 MeV/Nucleon," Yad. Fiz. **42** (1985) 1127–1137 [Sov. J. Nucl. Phys. **42** (1985) 712–718].

[15] S. Furihata, "Statistical Analysis of Light Fragment Production from Medium Energy Proton-Induced Reactions," Nucl. Instr. Meth. B **171** (2000) 252–258; "The Gem Code— the Generalized Evaporation Model and the Fission Model," Proc. MC2000, Lisbon, Portugal, 2000, edited by A. Kling, F. J. C. Barão, M. Nakagawa, L. Távora, and P. Vaz, Springer, Berlin, (2001), pp. 1045–1050; *The Gem Code Version 2 Users Manual*, Mitsubishi Research Institute, Inc., Tokyo, Japan (November 8, 2001).

[16] S. Furihata, K. Niita, S. Meigo, Y. Ikeda, and F. Maekawa, "The Gem Code—a Simulation Program for the Evaporation and Fission Process of an Excited Nucleus,"

JAERI-Data/Code 2001-015, JAERI, Tokai-mura, Naka-gam, Ibaraki-ken, Japan (2001).

[17] Shiori Furihata, "Development of a Generalized Evaporation Model and Study of Residual Nuclei Production," Ph.D. thesis, Tohoku University, March, 2003; S. Furihata and T. Nakamura, "Calculation of Nuclide Production from Proton Induced Reactions on Heavy Targets with INC/GEM," J. Nucl. Sci. Technol. Suppl. **2** (2002) 758–761.

[18] L. G. Sobotka, M. A. McMahan, R. J. McDonald, C. Signarbieux, G. J. Wozniak, M. L. Padgett, J. H. Gu, Z. H. Liu, Z. Q. Yao, and L. G. Moretto, "Compound-Nucleus Decay along the Mass-Asymmetry Coordinate and the Role of the Businaro-Gallone Point," Phys. Rev. Lett. **53** (1984) 2004–2007.

[19] R. J. Charity, M. A. McMahan, G. J. Wozniak, R. J. McDonald, L. G. Moretto, D. G. Sarantites, L. G. Sobotka, G. Guarino, A. Pantaleo, L. Fiore, A. Gobbi, and K. D. Hildenbrand, "Systematics of Complex Fragment Emission in Niobium-Induced Reactions," Nucl. Phys. A **483** (1988) 371–405.

[20] R. J. Charity, D. R. Bowman, Z. H. Liu, R. J. McDonald, M. A. McMahan, G. L. Wozniak, L. G. Moretto, S. Bardley, W. L. Kenoe, and A. C. Mignerey, "Emission of Complex Fragments from Highly Excited Systems Produced in ^{93}Nb+^{9}Be and ^{27}Al Reactions at $E/A = 25.4$ and 30.3 MeV," Nucl. Phys. A **476** (1988) 516–544.

[21] R. J. Charity, "$N - Z$ Distributions of Secondary Fragments and the Evaporation Attractor Line", Phys. Rev. C **58** (1988) 1073–1077.

[22] R. J. Charity, L. G. Sobotka, J. Cibor, K. Hagel, M. Murray, J. B. Natowitz, R. Wada, Y. El Masri, D. Fabris, G. Nebbia, G. Viesti, M. Cinausero, E. Fioretto, G. Prete, A. Wagner, and H. Xu, "Emission of Unstable Clusters from Yb Compound Nuclei," Phys. Rev. C **63** (2001) 024611; http://www.chemistry.wustl.edu/ rc/gemini/.

[23] N. Amelin, "Physics and Algorithms of the Hadronic Monte-Carlo Event Generators. Notes for a Developer," CERN Report CERN/IT/99/6, Geneva, Switzerland (1999); Web version of March 30, 2000, http://atlas.web.cern.ch/Atlas/GROUPS/SOFTWARE/OO/domains/ simulation/G4PhysicsStudies/documentation/ameline/makebookphysics.html; "GEANT4 Physics Reference Manual," June 22, 2005, http://wwwasd.web.cern.ch/wwwasd/geant4/ G4UsersDocuments/Overview/html/.

[24] L. G. Moretto, "Statistical Emission of Large Fragments: A General Theoretical Approach," Nucl. Phys. A **247** (1975) 211–230.

[25] W. Hauser and H. Feshbach, "The Inelastic Scattering of Neutrons," Phys. Rev. **87** (1952) 366–373.

[26] H. J. Krappe, J. R. Nix, and A. J. Sierk, "Unified Nuclear Potential for Heavy-Ion Elastic Scattering, Fusion, Fission, and Ground-State Masses and Deformations," Phys. Rev. C **20** (1979) 992–1013.

[27] P. Möller and J. R. Nix, "Nuclear Mass Formula with a Yukawa-Plus-Exponential Macroscopic Model and a Folded-Yukawa Single-Particle Potential," Nucl Phys. A **361** (1981) 117–146.

[28] A. J. Sierk, "Macroscopic Model of Rotating Nuclei," Phys. Rev. C **33** (1986) 2039–2053.

[29] K. T. R. Davies and A. J. Sierk, "Conditional Saddle-Point Configurations," Phys. Rev. C **31** (1985) 915–922.

[30] L. G. Moretto and G. J. Wozniak, "Multifragmentation in Heavy-Ion Processes," Ann. Rev. Nucl. Part. Sci. **43** (1993) 379–455.

[31] L. G. Moretto, K. X. Jing, L. Phair, K. Tso, and G. J. Wozniak, "Complex Fragment Emission from Low Energy Compound Nucleus Decay to Multifragmentation," Czechoslovak J. Phys. **45** (1995) 611.

[32] J. Toke and W. J. Swiatecki, "Surface-Layer Corrections to the Level-Density Formula for a Diffuse Fermi Gas," Nucl. Phys. A **372** (1981) 141–150.

[33] A. V. Ignatyuk, M. G. Itkis, V. N. Okolovich, G. N. Smirenkin, and A. S. Tishin, "Fission of Pre-Actinide Nuclei. Excitation Functions for the (α, f) Reactions," Yad. Fiz. **21** (1975) 1185–1205 [Sov. J. Nucl. Phys. **21** (1975) 612–621].

[34] P. A. Gottschalk and T. Ledergerber, "Shell-Correction Approach to Nuclear State Densities and the Competition Between Fission and Neutron Emission of ^{210}Po," Nucl. Phys. A **278** (1977) 16–44.

[35] J. P. Lestone, "Temperature Dependence of the Level Density Parameter," Phys. Rev. C **52** (1995) 1118–1121.

[36] J. Adam, A. Balabekyan, V. S. Barashenkov, V. P. Dzhelepov, S. A. Gustov, V. P. Filinova, V. G. Kalinnikov, M. I. Krivopustov, I. V. Mirokhin, V. S. Pronskikh, A. A. Solnyshkin, V. I. Stegailov, V. M. Tsoupko-Sitnikov, J. Mrazek, R. Brandt, W. Westmeier, R. Odoj, S. G. Mashnik, R. E. Prael, K. K. Gudima, and M. I. Baznat, "Study of Product Production from Proton-Induced Reaction on the ^{129}I Target at Proton Energy 660 MeV," Pis'ma v EChAYa, **1**, No. 4 [121] (2004) 53–64 [Particles and Nuclei, Letters, **1**, No. 4, 2004].

[37] Carmen Villagrasa-Canton, "Etude de la Production des Noyaux Résiduels dans la Réaction de Spallation Fe + p à 5 Énergies (300–1500 MeV/A) et Application au Calcul de Dommage sur une Fenêtre de Système Hybride," PhD Thesis, Universite de Paris XI Orsay, December 5, 2003, http://www-w2k.gsi.de/charms/theses.htm, and private communication from Dr. Villagrasa to SGM, March 11, 2004.

[38] C. Villagrasa, A. Boudard, J.-E. Ducret, B. Fernandez, S. Leray, C. Volant, W. Wlazlo, P. Armbruster, T. Enqvist, F. Hammache, K. Helariutta, B. Jurado, M. V. Ricciardi, K.-H. Schmidt, K. Sümmerer, F. Vivès, O. Yordanov, L. Audouin, L. Ferran, F. Rejmund, C. Stéphan, L. Tassan-Got, J. Benlliure, E. Casarejos, M. Fernandez, J. Pereira, S. Czajkowski,

D. Karamanis, M. Pravikoff, J. George, R. A. Mewaldt, N. Yanazak, M. Wiedenbeck, J. Connel, T. Faestermann, A. Heinz, A. Junghans, "Measurment of Residual Nucleus Cross Sections and Recoil Energies in p+Fe Collisions at 300, 500, 750, 1000, and 1500 MeV," Proc. ND2004, September 26–October 1, 2004, Santa Fe, NM, USA, edited by R. C. Haight, M. B. Chadwick, T. Kawano, and P. Talou, (AIP Conference Proceedings, Volume 769, Melville, New York, 2005), pp. 842–845.

[39] Paolo Napolitani, "New Findings on the Onset of Thermal Disassembly in Spallation Reactions," PhD Thesis, University Paris XI Orsay, IPNO-T-04-14, September 24, 2004, http://www-w2k.gsi.de/charms/theses.htm, and private communication from Dr. Napolitani to SGM, 2004.

[40] P. Napolitani, K.-H. Schmidt, A. S. Botvina, F. Rejmund, L. Tassan-Got, and C. Villagrasa, "High-Resolution Velocity Measurements on Fully Identified Light Nuclides Produced in ^{56}Fe + Hydrogen and ^{56}Fe + Titanium Systems," Phys. Rev. C **70** (2004) 054607.

[41] A. R. Balabekyan, A. S. Danagulyan, J. R. Drnoyan, G. H. Hovhannisyan, J. Adam, V. G. Kalinnikov, M. I. Krivopustov, V. S. Pronskikh, V. I. Stegailov, A. A. Solnyshkin, P. Chaloun, V. M. Tsoupko-Sitnikov, S. G. Mashnik, and K. K. Gudima, "Large Formation of Light Isotopes by Protons and Deuterons of 3.65 GeV/nucleon on Separated Tin Isotopes," LANL Report LA-UR-05-4676 (2005); E-print: nucl-ex/0506024; to be published in Yadernaya Fizika [Physics of Atimic Nuclei], 2006.

[42] G. Roy, L. Greeniaus, G. A. Moss, D. A. Hutcheon, R. Liljestrand, R. M. Woloshyn, D. H. Boal, A. W. Stetz, K. Aniol, A. Willis, N. Willis, and R. McCamis, "Inclusive Scattering of Protons on Helium, Nickel, and Tantalum at 500 MeV," Phys. Rev. C **23** (1981) 16711–1678.

[43] C.-M. Herbach, D. Hilscher, U. Jahnke,V. G. Tishchenko, J. Galin, A. Letourneau, A. Péghaire, D. Filges, F. Goldenboum, L. Penkowski, W. U. Schröder, and J. Tõke, "Charged-Particle Evaporation and Pre-Equilibrium Emission in 1.2 GeV Proton-Induced Spallation Reactions," Nucl. Phys. A **765** (2006) 426–463.

[44] Daniela Henzlová, "Systematic Investigation of the Isotopic Distributions Measured in the Fragmentation of ^{124}Xe and ^{136}Xe Projectiles," PhD Thesis, Chech Technical University in Prague, October 2005, http://www-w2k.gsi.de/charms/theses.htm.

[45] M. I. Baznat, K. K. Gudima, S. G. Mashnik, and R. E. Prael, "Merging the CEM2k and LAQGSM Codes with GEMINI," LANL Report LA-UR-05-0559, Los Alamos (2005), E-print: nucl-th/0501075, v2, November 2, 2005.

[46] K. Sümmerer and B. Blank, "Modified Empirical Parameterization of Fragmentation Cross Sections," Phys. Rev. C **61** (2000) 034607; K. Sümmerer, "Fragmentation Cross Sections Outside the Limiting-Fragmentation Regime," Nucl. Intr. and Meth. B **204** (2003) 278–281; http://www-w2k.gsi.de/charms/software.htm.

Distribution:
Eolus Team
R. B. Webster, X-DO, F644
M. B. Chadwick, X-1, PADNWP, B283
L. N. McClellan, X-DO, F645
J. A. Carlson, T-16, B28
J. S. Sarracino, X-1-SEC4, F663
S. C. Frankle, X-1-SEC3, F663
R. C. Little, X-1-SEC3, F663
J. D. Zumbro,X-1-SEC4, F663
E. J. Pitcher,LANSCE-DO, B243
G. W. McKinney, D-5, K575
L. S. Waters, D-5, K575
J. S. Hendricks, D-5, K575
M. R. James, D-5, K575
L. L. Hixson, ISR-CSSE, D466
K. K. Kwiatkowski, P-23, H803
X-DO file
T-DO file
T-16 file
X-3 file